SEABIRDS IN 3D: A FRAMEWORK TO EVALUATE COLLISION VULNERABILITY WITH FUTURE OFFSHORE WIND DEVELOPMENTS IN THE CALIFORNIA CURRENT SYSTEM

STEPHANIE R. SCHNEIDER[1], ELI WALLACH[2], CHARLES CHAMBERLIN[2], DAVID G. AINLEY[1], SCOTT B. TERRILL[1], SHARON H. KRAMER[1]*, R. GLENN FORD[3], JANET CASEY[3], JARROD A. SANTORA[4], LISA T. BALLANCE[5], SOPHIE B. BERNSTEIN[1], SADIE TRUSH[1], & ARNE JACOBSON[2]*

*[1]H. T. Harvey & Associates, 720 University Ave, Los Gatos, California, 95032, USA *(skramer@harveyecology.com)*
*[2]Schatz Energy Research Center, Cal Poly Humboldt, Arcata, California, 95521, USA *(arne.jacobson@humboldt.edu)*
[3]R. G. Ford Consulting Company, Portland, Oregon, 97232, USA
[4]NOAA Southwest Fisheries Science Center, Santa Cruz, California, 95060, USA
[5]Oregon State University, Newport, Oregon, 97365, USA

Received 15 September 2025, accepted 04 November 2025

ABSTRACT

Schneider, S. R., Wallach, E., Chamberlin, C., Ainley, D. G., Terrill, S. B., Kramer, S. H., Ford, R. G., Casey, J., Santora, J. A., Ballance, L., Bernstein, S. B., Trush, S., & Jacobson, A. (2026). Seabirds in 3D: A framework to evaluate collision vulnerability with future offshore wind developments in the California current system. *Marine Ornithology*, *54*(1), 215–240. http://doi.org/10.5038/2074-1235.54.1.1695

Since the 1970s, numerous vessel and aerial surveys of marine birds, covering many thousands of square kilometers, have been conducted in the California Current System (CCS), providing insights into seabirds' horizontal (2D) diversity and abundance, including the identification of "hotspots." Addressing knowledge gaps regarding seabird distribution patterns from a 3D (vertical) perspective, however, will be required if California (CA) is to use offshore wind (OSW) facilities to assist in reaching the state's 2045 renewable energy goals. Such an analysis will allow seabirds' vertical distribution to be considered when assessing potential OSW impacts, as collision vulnerability is greatest for birds flying at heights overlapping turbine rotor-swept zones (RSZ). This probability is determined by the interaction of species-specific morphology and flight-style with wind speed. Thus, predicting the proportion of seabirds moving at RSZ heights can be achieved by quantifying: (1) the likelihood that significant numbers of individuals of various species, of those present, will reach RSZ heights across the full spectrum of wind speeds, (2) species-specific density in 2D space, and (3) the windscape. To address these goals, we describe a novel 3D Seabird Collision Vulnerability Framework (3D Framework) that integrates historical at-sea observations with the offshore windscape to predict the densities of 44 species with sufficient sample sizes to support a 3D assessment of their expected distribution below versus within RSZ heights. The prediction region encompasses all offshore waters capable of supporting current OSW mooring technologies, which, in CA and southern Oregon, includes waters overlying the continental shelf and upper continental slope. This 3D Framework can be modified to incorporate new data and new locations as the OSW industry expands. This effort supports the broader goal of identifying sites within the CCS that optimize power generation while minimizing interactions with seabird species whose flight behavior makes them vulnerable to collision.

Key words: density, flight height, occurrence patterns, seabirds, offshore wind energy

LIST OF ABBREVIATIONS AND ACRONYMS

2D – two-dimensional planar space (e.g., latitude and longitude); **3D** – three-dimensional space including vertical dimension (e.g., altitude); **3D Framework** – *Seabirds in 3D: A Framework to Evaluate Collision Vulnerability With Future Offshore Wind Developments*; **ASL** – above sea level; **BOEM** – Bureau of Ocean Energy Management; **CA** – California; **CCS** – California Current System; **CEC** – California Energy Commission; **CUTI** – Cumulative Upwelling Transport Index; **EEZ** – Exclusive Economic Zone; **EQN** – equation; **ESA** – Endangered Species Act; **FG** – flight-style groupings; **GW** – gigawatts; **IDW** – inverse distance weighting; **km** – kilometers (1 km ≈ 0.6 miles); **LOO-CV** – leave-one-out cross-validation; **m** – meters (1 m ≈ 3 feet); **m/s** – meters per second (1 m/s ≈ 0.514 knots); **NREL** – National Renewable Energy Laboratory; **OCS** – outer continental shelf; **OR** – Oregon; **OSW** – offshore wind; **Project** – California Energy Commission project titled *Seabirds in 3D: A Framework to Evaluate Collision Vulnerability With Future Offshore Wind Developments* (including the Optimization Analysis); **RSZ** – rotor-swept zone; **SB** – Senate Bill; **WEA** – wind energy areas.

INTRODUCTION

Context and Background

To achieve the goal of powering CA with clean, renewable energy by 2045, in accordance with the 100% Clean Energy Act of 2018 (SB 100) (*California Senate Bill 100*, 2018), the state will need to diversify energy sources. OSW stands out as a cost-competitive resource (Rose et al., 2022) with the potential to contribute significantly to meeting SB 100 targets. The windscape across CA's coastal and OCS regions, characterized by seasonally strong winds, is highly favorable for OSW electricity generation. In alignment

with SB 100, the CEC has outlined plans to achieve 2–5 GW of OSW capacity by 2030, with an ambitious increase to 25 GW by 2045 (Flint et al., 2022).

The successful deployment of OSW facilities, however, necessitates thorough environmental assessment, permitting, and construction and operational planning. In particular, the permitting and siting of floating OSW facilities will require better understanding of potential impacts on marine communities, including the avifauna, especially species associated with the deeper OCS waters. The latter species are not typical of OSW facilities in the Atlantic, where much data on impacts has been amassed. Many seabird species that frequent windy regions like those of the CCS engage in a flight-style known as "dynamic soaring," which uses the wind in a repeating cycle to gain altitude, after which gravitational energy is used to make forward progress, doing so with little, if any, wing beating (Ainley et al., 2015; Pennycuick, 1987a, 1987b). Wind energy is as important as food energy to these species.

Decades of at-sea surveys and their analyses have provided a baseline understanding of the spatial diversity and abundance of seabirds across the CCS, exclusively in 2D (e.g., Adams et al., 2014, 2016; Ainley & Hyrenbach, 2010; Briggs et al., 1987; Ford et al., 2021; Joyce, 2016; Kelsey et al., 2025; Leirness et al., 2021; Mason et al., 2007; Nur et al., 2011; Russell et al., 2023; see Appendix A, Table A1, available on the website). These efforts have focused on identifying seabird activity "hotspots." However, the resulting seabird maps lack a vertical component.

Despite the insights gained from 2D predictions, which may be used to shift OSW areas away from seabird "hotspots" (e.g., Leirness et al., 2021), most seabird fatalities from OSW development are expected to result from collisions with rotating turbine blades. These blades are elevated well above the sea surface (~25–30 m above sea level [ASL]) at the lowest sweep of their rotation. To assess seabird collision risk, it is crucial to consider flight altitudes, relative to RSZs, of species overlapping potential OSW development. Accordingly, increasing the dimensionality of predictions from 2D to 3D is imperative for a more accurate understanding of the vulnerability of the CCS seabird community to RSZ collisions.

Previous attempts to model seabird communities have lacked a vertical dimension because few at-sea surveys have estimated flight altitude of the seabirds encountered. Estimating precise and accurate bird altitude ASL is challenging, particularly because most seabird observations have been made from low-lying vessels at or near the sea surface. Consequently, the precision and accuracy of such estimates diminish with increasing vertical distance between observers and seabirds (Cook et al., 2018; Harwood et al., 2018; Largey et al., 2021; Webb & Nehls, 2019).

Additionally, prior 2D assessments—not only off CA but in most regions—have provided only relative metrics of abundance (e.g., Adams et al., 2016; Kelsey et al., 2025; Leirness et al., 2021), owing to a lack of adjustment for seabird movement relative to observer movement (i.e., flux-corrected counts; Spear et al., 1992). Such corrections allow determination of actual seabird density. Importantly, some historical at-sea counts can now be adjusted for flux to estimate density using procedures described by Clarke et al. (2003), provided that vessel speed and direction, as well as bird speed and direction (see Spear & Ainley, 1997a, 1997b), are logged. Several CCS at-sea surveys have collected these data (DODS, EPOC, GOED, JVRK, RUWE; Appendix A, Table A1). Various methods exist to generate 2D density predictions, and a framework with CCS-specific data is already available to predict seabird flight height based on FG and wind speed (Ainley et al., 2015). Thus, it is now possible to begin predicting the composition and density of CA's seabird community at heights overlapping RSZs.

As the OSW industry expands into deeper waters where wind farms have not yet been sited, there is a growing need to understand the potential impacts on seabird populations occupying these habitats. This necessitates investigations of the composition and density of birds flying at heights overlapping RSZs, particularly in comparison with shallower near-coastal waters where OSW facilities currently operate in the Atlantic. Initiating development of a predictive framework for seabird composition and density at altitudes intersecting RSZs in the CCS represents a crucial first step. Such a framework would provide valuable insights to help identify sites with reduced presence of dynamic soaring and other seabirds that enter the RSZ. This information would be instrumental in facilitating the environmental permitting process for floating OSW facilities off CA. Furthermore, advances in technologies for monitoring seabird movements in remote offshore environments offer the potential to substantially enhance the precision and reliability of predictions generated through such a framework (e.g., Schneider et al., 2024).

Purpose and Goals

The purpose of this 3D Framework study was to predict the 2D and 3D density of the 44 most abundant seabird species across areas capable of supporting OSW mooring infrastructure between Point Conception, southern CA, and Yaquina Head, central OR. Waters south of Point Conception were not included because no OSW is proposed. Leveraging datasets of the offshore seabird community and windscape collected over recent decades, the results contribute to the broader Project goal of implementing a multi-objective optimization to identify sites that simultaneously minimize seabird collision vulnerability and maximize energy generation (Fig. 1).

METHODS

Overview of the 3D Framework

The 3D Framework is best conceptualized as a multi-component analysis (Fig. 2):

Component I: Relate Flight Heights to Wind Speed

The CCS's diverse seabird community is divided into distinct FGs, unified by relatively homogenous taxonomy and morphology (Ainley et al., 2015; see also Spear & Ainley, 1997a, 1997b). FG-specific probability curves, which indicate the chance of a bird overlapping RSZs across the full spectrum of wind speeds that typify the CCS (0–30 m/s), given its FG, were generated using a mixed-effects logistic regression based on an extensive seabird flight-height behavior dataset.

Component II: Predict Densities in 2D

Observational seabird data were partitioned into one of three oceanographic seasons, each with distinct wind-driven upwelling and temperature regimes: Upwelling, Oceanic, or Davidson Current (e.g.,

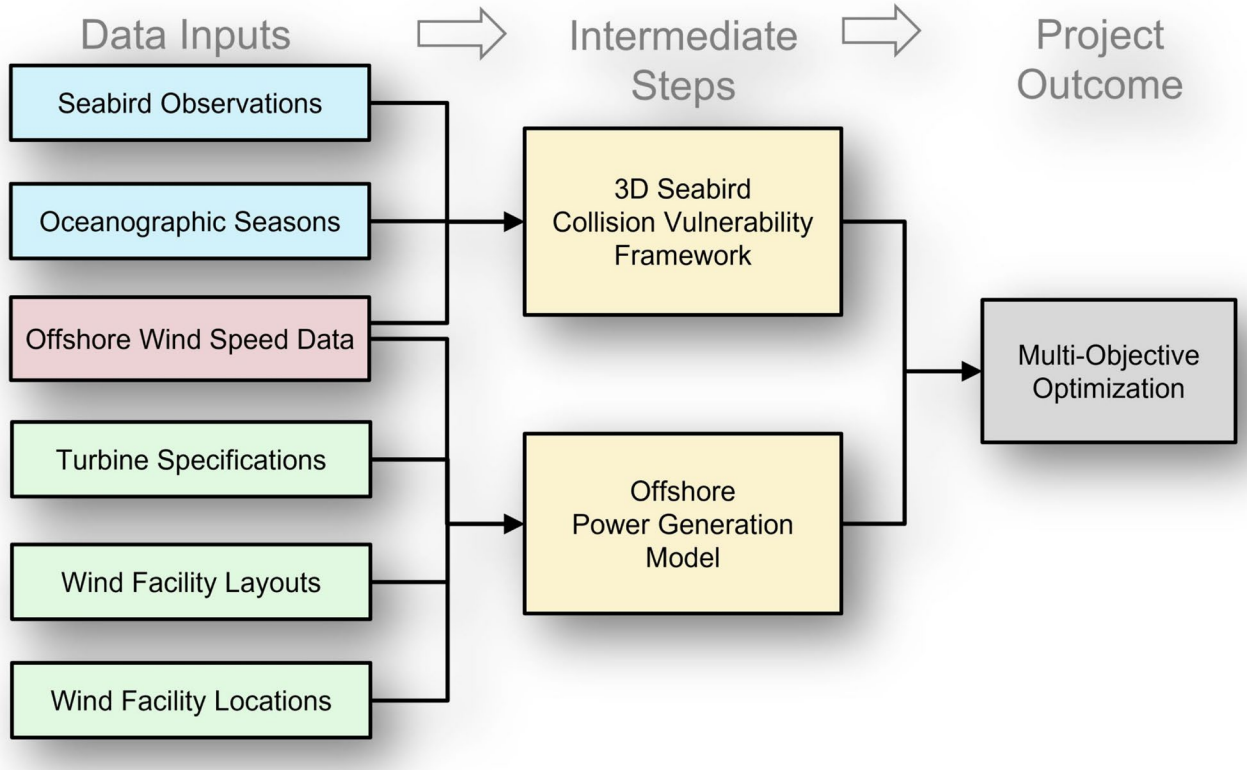

Fig. 1. Diagram of the 3D Seabird Collision Vulnerability Framework integrated into the broader Multi-Objective Optimization Framework of the 3D Project. The 3D Framework (upper yellow box) is one integral part of the broader Multi-Objective Optimization Framework of this more comprehensive Project, aimed at quantitatively evaluating offshore power generation capacity while minimizing seabird collision risks (grey box). This overarching objective relied on two intermediate assessments (yellow boxes): the 3D Seabird Collision Vulnerability Framework, the focus of this paper, and an Offshore Power Generation Model, detailed in a separate report (https://schatzcenter.org/publications/). Data inputs supporting these assessments were color-coded as being either specific to the 3D Seabird Collision Vulnerability Framework (blue boxes), the Power Generation Model (green boxes), or used by both (pink boxes).

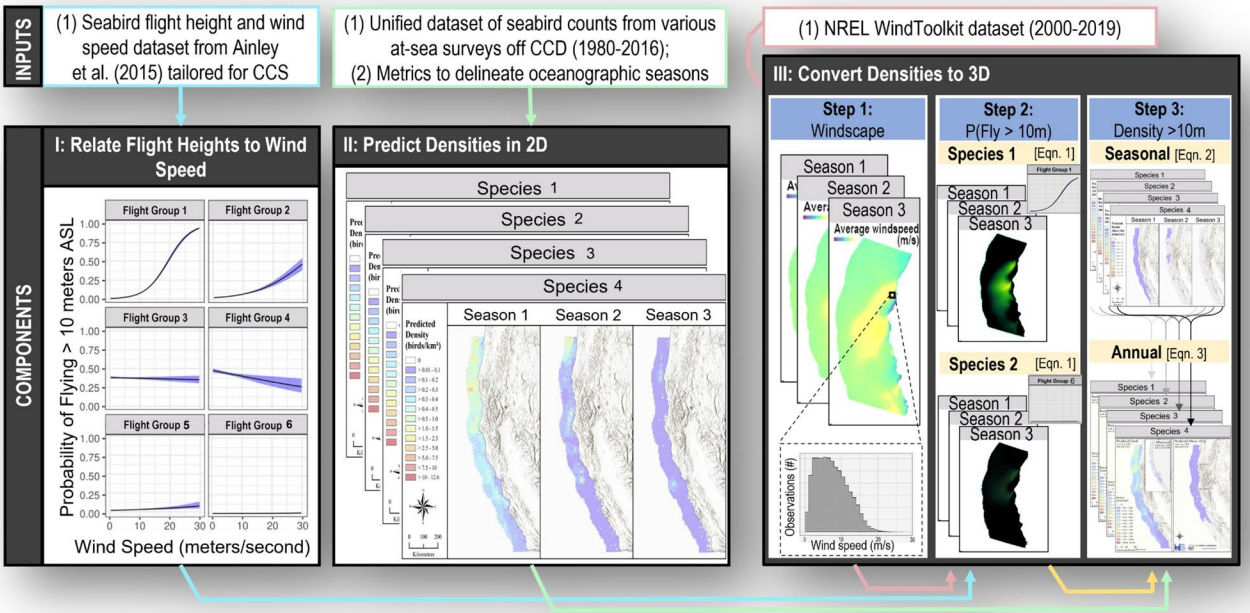

Fig. 2. Analysis components of the 3D Seabird Collision Vulnerability Framework. The flowchart illustrates how diverse data were input and integrated across the three analysis components to generate annual predictions of 3D density (birds/km^2) for the California (USA) Current System (CCS) seabird community. Each panel corresponds to a distinct component, and colored arrows depict data flow and connections between components.

Bolin & Abbott, 1963; Chelton et al., 1982; Hickey, 1979). Traditional 2D density predictions were made at regularly spaced (i.e., gridded) intervals for each species and season using a spatial interpolation algorithm (see Supporting Data section under Component II methods for study details). To evaluate the accuracy of the 2D density predictions (birds/km^2), a cross validation was used to assess how effectively the spatial interpolation algorithm captured underlying patterns and made predictions for new, unseen data.

Component III: Convert 2D Densities to 3D

Using outcomes of Components I and II, the dimensionality of 2D density predictions was increased to create a 3D representation of the seabird community. This required the following steps: (S1) for each grid location having a 2D density prediction, a comprehensive distributional representation of the windscape (including extremes) was generated for each season; (S2) this gridded windscape was then integrated with the outcome of Component I to derive seasonal-, site-, and FG-specific probabilities of being at collision risk height; and (S3) probabilities from S2 were then applied to the outcome of Component II to vertically partition overall density estimates and isolate the predicted density at collision risk height.

Spatially explicit 2D and 3D density predictions were aggregated across seasons and species and subsequently visualized using GIS mapping. The annual prediction maps represent expected patterns based on a long-term, multi-decadal perspective of the seabird community across the CCS rather than the extremes of abundance that may occur in individual years. This perspective is intended to facilitate OSW permitting and siting. Although such extremes can be important, the resources required to address this perspective were beyond the scope of this study, particularly given substantial interannual variability and ongoing changes in marine bird populations (e.g., Ainley & Hyrenbach, 2010; Grémillet et al., 2018; Paleczny et al., 2015; Veit et al., 1997).

Component I: Flight Heights and Wind Speed

Probabilities of seabirds flying at heights associated with collision risk (i.e., > 10 m) were computed across a range of OSW speeds (0–30 m/s), encompassing wind speeds required for turbine rotation (3–25 m/s; Severy et al., 2020) and representative of conditions in the CCS. These probability estimates were derived from data specific to seabirds in the CCS, based on a comprehensive assessment covering a significant portion of the eastern Pacific Ocean, which includes the CCS (Ainley et al., 2015). Key assumptions and definitions used in this analysis are outlined below.

The CCS seabird community was simplified into various distinct FGs following Ainley et al. (2015). Results presented here focus on FGs of the CCS species abundant enough to offer sufficient information for Components I, II, and III of the 3D Framework.

Birds vulnerable to collision were those that frequently fly at heights of 10 m or greater. Although this threshold includes airspace below the lower extent of typical OSW RSZs, which is typically at ~25–30 m ASL, this vertical mismatch could not be avoided because of the way flight-height data were originally collected. Observations were made from vessels by observers stationed at an eye-height of ~10–12 m ASL, and all birds above 10 m were assigned to the same flight-height bin, regardless of whether they were at 10 m or 50 m, or higher. Data for analogous species outside the CCS, where actual flight heights were recorded, indicate that birds in this category do frequently fly within RSZs. Thus, until flight-height estimates can be improved and made more specific to the CCS (e.g., Matzner et al., 2022; Schneider et al., 2024), the 10 m threshold serves as a proxy for seabirds achieving heights at which they are likely to overlap RSZs.

Supporting Data

To generate probability curves of seabirds flying at RSZ height for various FGs and wind speeds, an extensive dataset collected on a series of cruises between 1976 and 2006 was used (Appendix A, Table A1). The original database contained relevant information on 131,354 individuals of 271 species across the Pacific Ocean, inclusive of the CCS, the equatorial Pacific off Hawai‘i, the Humboldt Current off South America, and the Southern Ocean, as detailed in Ainley et al. (2015). An appreciable number of species observed in those areas also travel to the CCS (see, e.g., Howell & Zufelt, 2019). To support a CCS-specific analysis, this more extensive dataset was filtered to retain all observations from the CCS, as well as records of species known to be present off CA but also observed elsewhere (e.g., Laysan albatross *Phoebastria immutabilis* in the Equatorial Pacific). For a comprehensive description of the original data collection protocols, refer to Ainley et al. (2015).

A crucial aspect of these data collection initiatives involved categorizing flight heights for all seabird observations into the following predefined categories: on the sea surface or foraging (i.e., remaining in one place); flying 0–3 m ASL; flying > 3–10 m ASL; or flying above 10 m ASL.

Including birds on the sea surface, for which flight height equaled 0 m ASL, was essential for deriving an overall 2D representation (Component I), because the standardized seabird observation database used to derive 2D density estimates included both flying and stationary birds. As such, accounting for birds on the sea surface was crucial for partitioning 2D densities before converting to 3D.

Logistic Regression

The predicted probability of flying > 10 m for each of the 18 FGs that contained a sufficient sample size for further statistical analysis was calculated using a mixed-effect logistic regression. The *glmer* function in the “lme4” package in R (Bates et al., 2015) was used, with wind speed as a fixed effect and FG as a random effect. FG was treated as a random effect to account for correlated structures (Midway, 2022), given that the species modeled are part of a larger seabird population (Li et al., 2011). Final plots with wind speed as a predictor versus the probability of the binary response were generated for each FG using the outcome of this analysis, with confidence intervals around each probability curve generated via non-parametric bootstrapping.

Component II: Seabird Densities in 2D

Our primary goal was to apply the 3D Framework to a large marine region inclusive of areas that could support future OSW facilities. Consequently, our study area included CA’s Humboldt and Morro Bay WEAs, which have already been leased to floating OSW developers (BOEM, 2022). We also included seabird observations from central and southern OR, as the regional avifauna extends into these areas; this expanded the sample size and improved predictions

for northern CA's seabird community. Other WEAs are under consideration within the region but have not yet been finalized.

Area of Interest

Seabird observations supporting Component II of the 3D Framework encompassed all continental shelf waters from Point Conception, CA, to Newport, OR (34.40°N to 44.74°N), extending offshore to 370 km (essentially the U.S. Exclusive Economic Zone) (-120.40°W to -131.0°W) (Fig. 3). Predictions were generated in 2D and 3D for a specific subset of this area, extending 80 km perpendicular to the coastline (Fig. 3). This focused prediction region was selected because it was inclusive of all waters shallow enough to support the current state-of-the-art floating OSW mooring infrastructure defined by BOEM and NREL (i.e., the upper OCS, no more than 1,300 m deep). The depth of 200 m represents the continental shelf break, beyond which slope waters deepen to 3,000 m to the west (i.e., the OCS). The upper portion of the slope (< 1,300 m) is the primary area currently leased for OSW development. The seabird prediction space was divided into a uniform grid of 1,806 cells, each with a 2D dimension of 5-min latitude by 5-min longitude, and seabird community predictions were generated for each grid cell.

In addition, to assess differences in the composition of California's seabird community (the average annual density estimates [birds/km^2] for broadly grouped taxa) from 2D (all elevations) and 3D (> 10 m) perspectives, the study area was divided into six regions. Cape Mendocino (40.44°N) served as the boundary between north-south divisions, which were further defined by distance from the coastline. These divisions also considered offshore wind facility jurisdiction, resulting in two main categories: "State," representing waters under CA or OR jurisdiction that extend out to 4.8 km (i.e., 3 mi); and "Fed (Federal)" representing waters beyond this limit. Within "Fed" waters, two additional subdivisions were made: "None," for areas not currently considered for wind energy development (4.8–32 km offshore), and "WEAs," representing the western extent of waters off CA physically capable of supporting offshore wind moorings (i.e., < 1,300 m; 32–80 km offshore), including all currently leased WEAs.

Supporting Data

At-Sea Seabird Studies. To facilitate 2D density predictions for Component II, seabird observations were compiled from across the CCS, including cruises from which observations used to derive Component I flight-height and wind speed probability curves were obtained. The dataset for Component II was collected from nine systematic aerial and vessel-based strip-transect surveys conducted in waters off CA and OR between 1980 and 2016 (Table 1; Appendix A, Table A1). Effort associated with these studies varied in terms of annual and seasonal coverage (Table 1), spatial coverage (Fig. 4), and total survey effort across the study area (Fig. 5).

Data Standardization Across Studies. Although the various surveys employed a range of methodologies, they all adhered to continuous strip-transects typical for at-sea surveys of seabirds (Spear et al., 1992, 2004). At least one, but more often two, observers recorded all birds detected from a moving platform; identifications were made to the lowest feasible taxon, and associated counts were recorded. Additional details on survey protocols are available through the references listed in Appendix A, Table A1.

One important difference in survey protocols was the width and segment length of census strips, with the most pronounced difference occurring between the strip-width associated with aerial surveys (50–75 m) and vessel surveys (300 m; Appendix A, Table A1). This difference was a result of platform speed and the ability of observers to count every bird in their strip. On aircraft flying at 100 knots (182 km/h), only 50–75 m could be accommodated, compared to 300 m on vessels moving at 12–15 knots (22–28 km/h). To account for this difference in effort per length of transect travelled, continuous strip-transect results were standardized to a common format. Specifically, each transect line was divided into 1 km^2 units of survey effort, representing areas of equal transect effort. These 1 km^2 segments could be better accommodated in the 5′ × 5′ grid cells. This standardization ensured that spatial efforts associated with counts were approximately equal, allowing observations from multiple surveys to be combined.

Once all the datasets were harmonized and counts were expressed in terms of equivalent survey effort, they were corrected to account for flux related to the movement direction and speed of seabirds relative to the movement direction and speed of observers, following methods explicitly described by Spear et al. (1992) and validated by studies comparing estimates from flux-corrected counts of seabirds to adjacent, well-censused seabird colonies (e.g., Clarke et al., 2003; Ford et al., 2021; Russell et al., 2023). For birds moving too slowly for double-counting to be a concern, including stationary birds (e.g., birds resting on the water or foraging (diving, plunge diving, dipping, surface seizing), flux is negligible, and observed counts are effectively equivalent to flux-corrected counts.

Oceanographic Seasons

Seabirds exhibit strong responses to changes in productivity and food availability (Ainley et al., 2005), driven by seasonally variable conditions that characterize the CCS and are not captured in conventional calendar-based seasons—namely the Upwelling, Oceanic, and Davidson Current periods. Winds and productivity differ among these periods, as noted above. In recognition of this, the 3D Framework generates species-specific predictions for each oceanographic season. By partitioning seabird observations to better align with shifts in seasonal productivity of the CCS, the 3D Framework is intended to be sensitive to, and capture, corresponding shifts in seabird distribution and density across the region over a typical annual cycle. For each of the three CCS-specific oceanographic seasons (Fig. 6), the key characteristics and methods applied to identify approximate start and end dates are described in the following subsections, generally based on multi-decadal ocean climate records. However, these CCS seasons do not fully capture the seasonal presence of many seabird species that nest in the Southern Hemisphere and visit the CCS during their non-breeding season (Ainley, 1976; Briggs et al., 1987), although their occurrence may overlap temporally with one or more of the three CCS seasons.

Upwelling Season. This season is characterized by the upward transport of cold, nutrient-rich water to the sea surface, which supports phytoplankton blooms (Bolin & Abbott, 1963; Checkley & Barth, 2009). Increased phytoplankton availability, in turn, fuels the development of the entire food web, from grazers to various levels of predators, synchronizing with seabird nesting along the CA coast (Ainley & Boekelheide, 1990; Ainley et al., 2005; Nur et al., 2011).

The commencement of this season has traditionally been marked by the "Spring Transition," a period after winter when prevailing winds

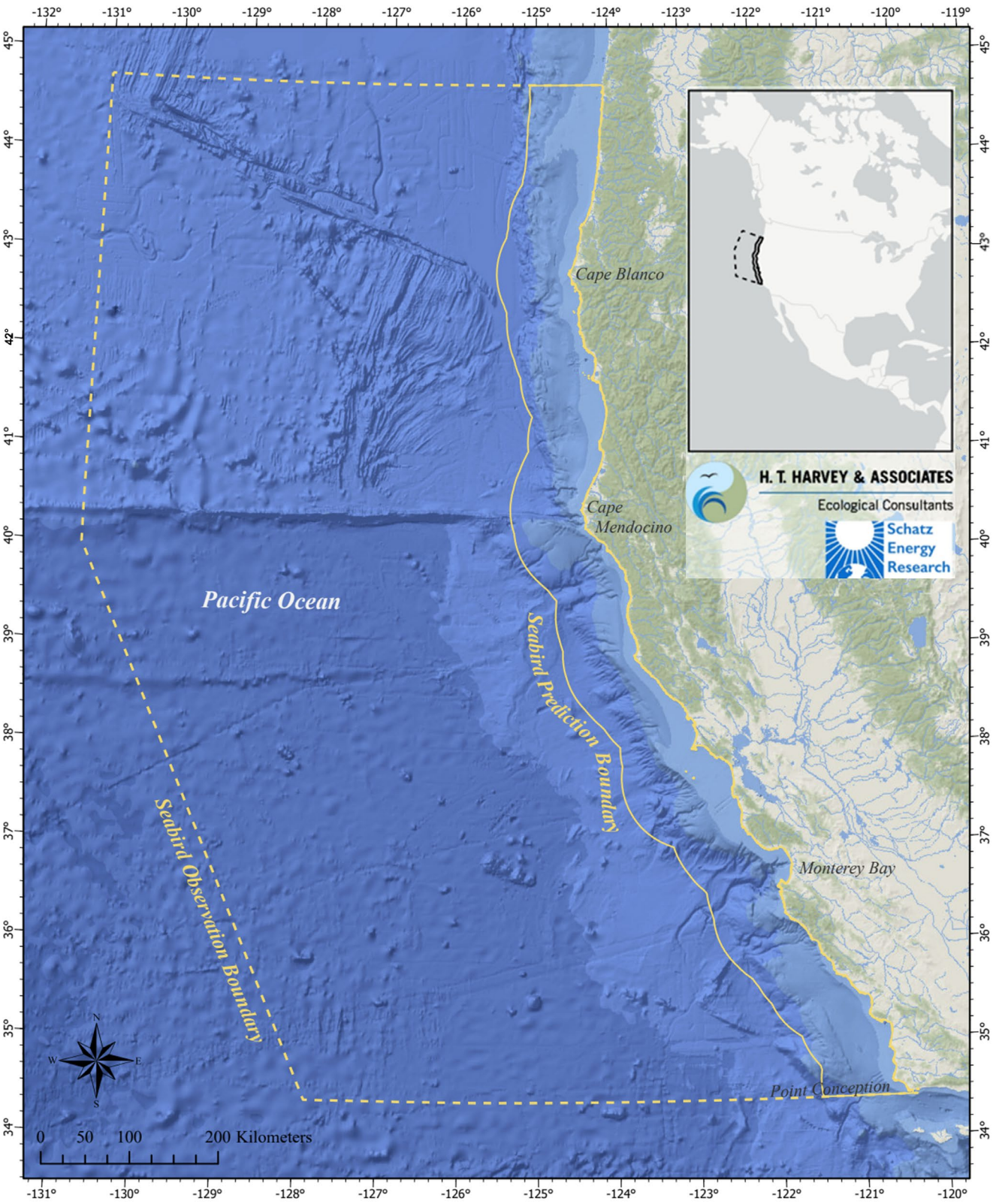

Fig. 3. Seabird observation and prediction boundaries. The seabird observation boundary (dashed yellow line) delineates the entire area for which seabird observations were amassed and standardized. This observation boundary encompassed the U.S. Exclusive Economic Zone. In contrast, the seabird prediction boundary (solid yellow line) delineated the more focused spatial extent of 2D and 3D density predictions, which includes all areas being considered for offshore wind development in California. Map includes Oregon and California coastlines, USA.

shift from the south to the northwest, leading to upwelling and a sharp drop in sea surface temperature. Changes in along-shelf winds, in combination with the Coriolis effect, shift surface waters from downwelling-dominant to upwelling-dominant. This transition can

TABLE 1
At-sea surveys supporting component II of the 3D Seabird Collision Vulnerability Framework

Survey[a]	Type[b]	State	Years	Area Surveyed (km²)			
				Upwelling	Oceanic	Davidson	Total
CNCA	A	CA	1980–83	2,015	1,456	930	4,401
OSPR	A	CA	1994–97 2001–12 2014 –16	2,920	2,525	1,594	7,039
PSEA	A	OR	2011–12	641	657	661	1,959
DODS	V	CA	1995–2001	1,634	990	381	3,005
EPOC	V	CA	1983 1985–86, 1988–92, 1994–95	118	55	207	380
GOEO	V	CA/OR	2000-02	1,989	147	0	2,136
JVRK	V	CA	1997–2006	2,712	0	0	2,712
OCWA	V	CA/OR	2001 2005 2008 2014	901	3,407	300	4,608
RVWE	V	OR	2005	79	0	0	79
ALL	Both	CA/OR	1980–2016	13,009	9,237	4,073	26,319

[a] See Appendix A, Table A1 for code definitions
[b] A, aerial; V, vessel

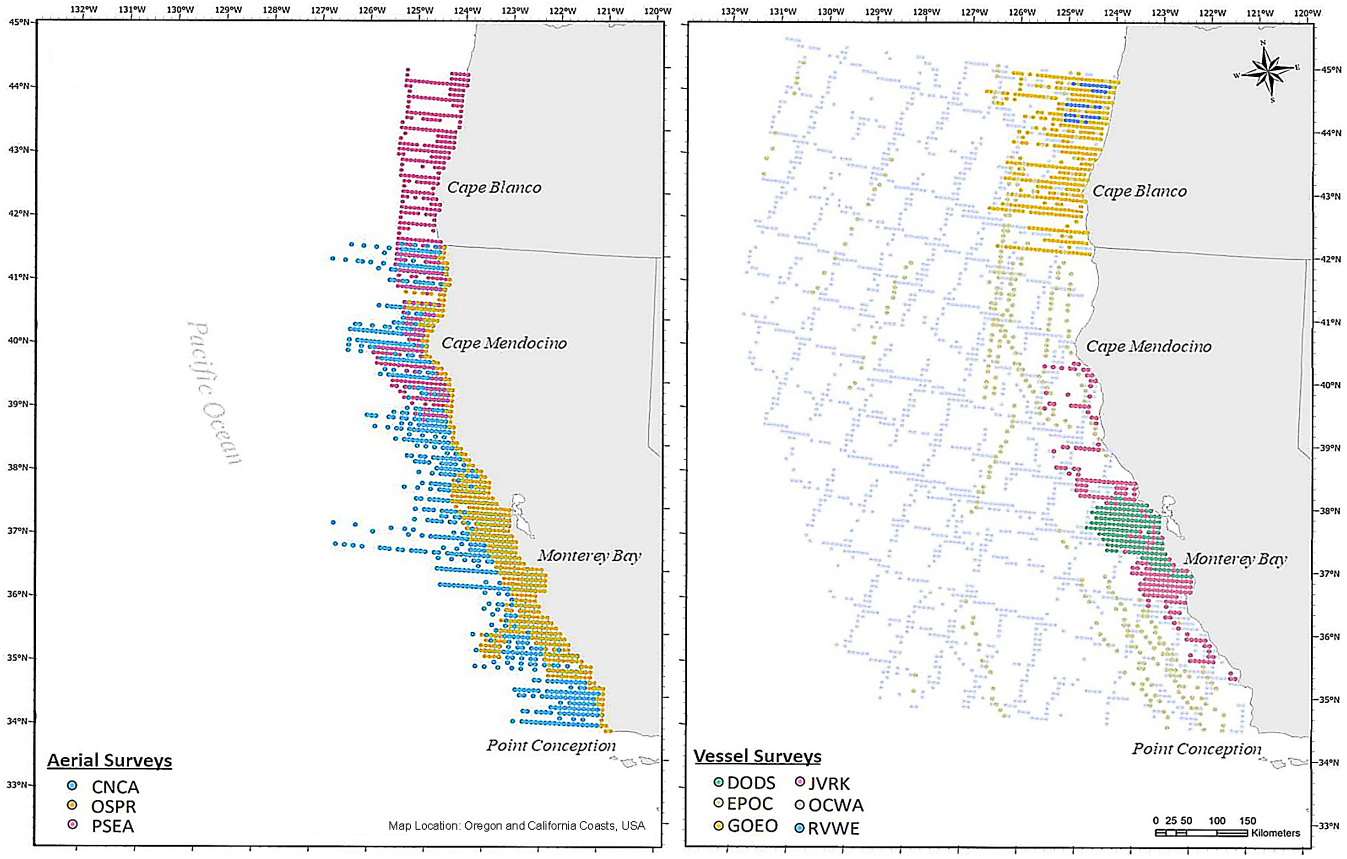

Fig. 4. Aerial and vessel survey center points. Center points of each 1 km² Survey Effort Unit within the three aerial (left panel) and six vessel (right panel) surveys used in this project. See Table 1 and Appendix Table A1 for data source definitions.

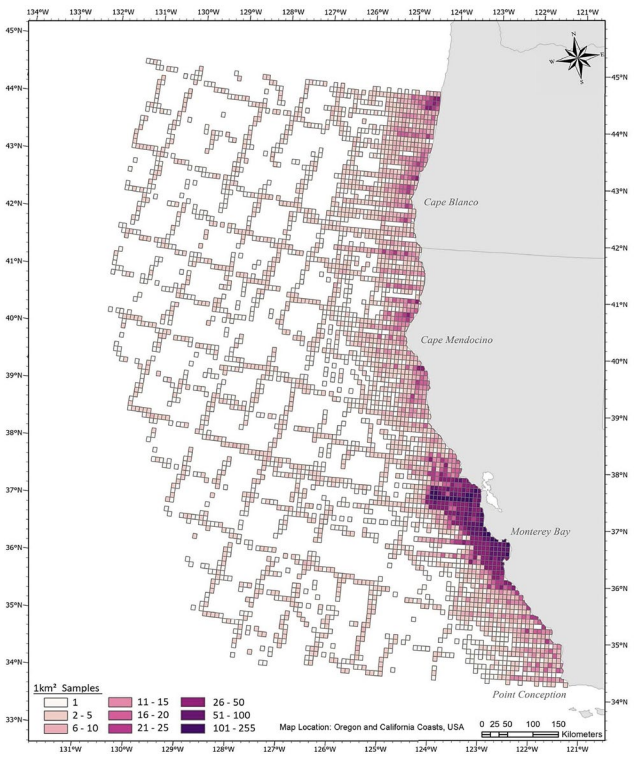

Fig. 5. Distribution of survey effort across the entire study area. Survey effort was quantified by summing the total number of 1 km^2 units of at-sea survey effort, aligned with the resolution of the 2D and 3D prediction grid (5′ × 5′ cells). The intensity of survey effort at each location is depicted using a color gradient, with darker shades indicating areas of greater survey coverage.

be identified by the shape of the Cumulative Upwelling Transport Index (CUTI) curve, specifically at the inflection point, indicating that upward transport of deep water has become predominant. The timing can vary by up to two months, with repercussions to the food web and the seabird community (Ainley & Boekelheide, 1990; Ainley & Hyrenbach, 2010).

While the Spring Transition occurs earliest in the south and shifts northward as time proceeds, we used the average date of this CUTI inflection point for latitudes between 33°N and 45°N over a 40-year period (1967–2007), as determined by Bograd et al. (2009), for the entire study area.

Based on the last few decades, the Upwelling season extends from 25 February to 13 August, totaling 170.25 days (the 0.25 represents an extra day added to February every fourth year). Again, upwelling begins earlier in the south than in the north of the study area.

Oceanic Season. This season is characterized by the weakening of northwesterly winds, reducing the upwelling of cold, dense water to the surface to be displaced at the surface by warmer, subtropical waters that intrude from the west. Intrusion of these warmer waters, sometimes called "tuna water," was tracked using the position of the 17.5°C isotherm, which is the ocean boundary along which the troll fishery operates for Albacore *Thunnus alalunga*.

The commencement of this season was determined by tracking the seasonal progression of the 17.5°C isotherm using NASA's State of the Ocean Worldview visualizer over a 19-year period (2002–2021). The isotherm maintained a consistent position far offshore during the Upwelling season, then shifted substantially eastward to varying degrees depending on year into a relatively nearshore position,

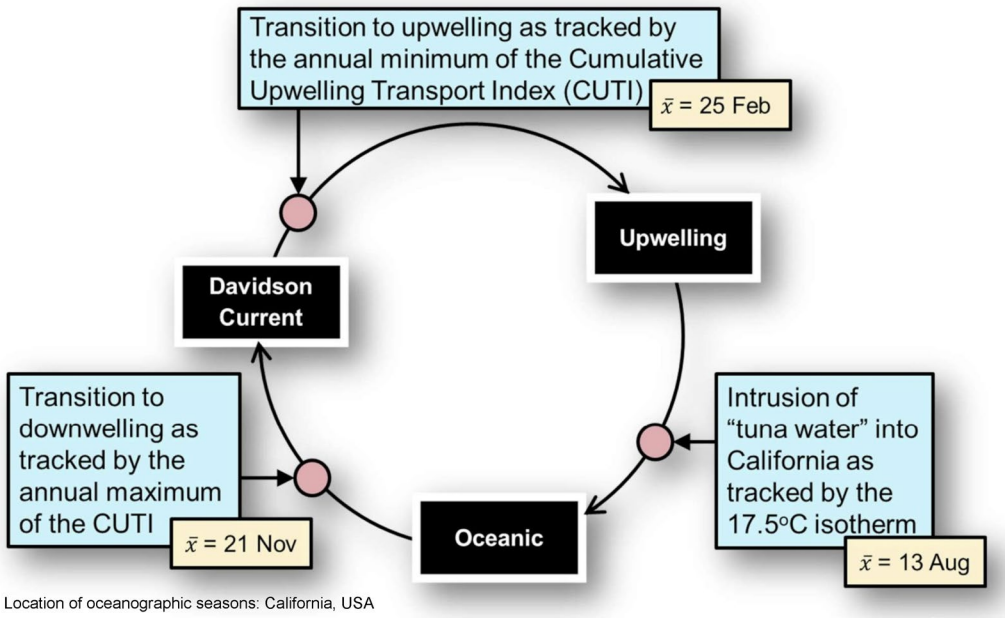

Fig. 6. California (USA) Current System (CCS) oceanographic seasons. The annual cycle of the CCS was partitioned into three oceanographic seasons (Upwelling, Oceanic, and Davidson Current), each characterized by distinct ocean climates and associated with different seabird community compositions (see Bolin & Abbott, 1963; Chelton et al., 1982; Hickey, 1979). Yellow boxes indicate season initiation dates, while blue boxes represent the commencement criteria. For the Upwelling season, the diagram indicates that the average onset occurs on 25 February, as determined by the annual minimum of the Cumulative Upwelling Transport Index curve (Bograd et al., 2009).

marking the beginning of the Oceanic season. This season extended from 14 August to 20 November, totaling 99 days.

Davidson Current Season. This season is characterized by the surfacing of the Davidson Current, normally an undercurrent flowing counter to the California Current. Southerly winds, especially from winter storms, allow this warmer, low productivity current to surface. The commencement of this season was based on the 40-year average of CUTI's deflection point, contrasting with the inflection point used for the Upwelling season (Bograd et al., 2009). This season extended from 21 November to 24 February, totaling 96 days.

Inverse Distance Weighting

The 2D density predictions were derived using an interpolation technique known as Inverse Distance Weighting (IDW). Specifically, weights assigned by IDW are inversely proportional to the distance between the observed point and the prediction point, hence the name "Inverse Distance Weighting." Using the IDW algorithm, density estimates (birds/km^2) for each species-season combination were generated across the seabird prediction area (see Fig. 3) for each of the 1,814 5′ × 5′ cells. Once estimates were generated, 2D density observations and predictions could be visualized for all seabird taxa as maps matching the resolution of this seabird prediction grid.

The general process for estimating the density of seabirds using IDW was as follows:

Step 1: Create IDW Input Database. Details regarding the extensive seabird dataset amassed were summarized for each species included in the 3D Framework (see Appendix A, Table A2). To make targeted predictions of 2D seabird density into regions with significant effort and potential for OSW development using IDW, these extensive observation datasets were truncated to only include observations up to 83 km from the coastline. These observations were further segmented by oceanographic season, with each iteration of the IDW algorithm processing a single species-season combination.

Step 2: Calculate Observed Densities for Each Species-Season Combination. Observed density datasets created in Step 1 were averaged within the highest-resolution grid supported by the input data (i.e., a 1 km × 1 km grid, equivalent in area to the standardized unit of effort for the input data). Each grid cell was assigned a single density value representing the average density of all survey points within that cell. Cells with zero bird densities for a given season-species combination, where surveys had occurred, were treated as true zeros (i.e., no birds detected) and were retained as valid inputs for the IDW algorithm. In contrast, cells lacking observation data because they were not surveyed were treated as missing data rather than valid count data and therefore required interpolated density estimates.

Step 3: Apply IDW Algorithm. Due to the reliance on distance metrics for IDW interpolation, input data were treated as point estimates, as opposed to polygons, to make the necessary distance calculations. Using the average observations for each IDW grid cell centroid and the distances to cell centroids for which density estimates were computed, seabird density was estimated for each species and season. These estimates were used to populate the 5′ × 5′ grid associated with the seabird prediction area using the following IDW expression (EQN 1):

$$B(x,y) = \frac{\Sigma_{obs}\, b_{obs} \times \left(\frac{1}{d_{obs}}\right)^{IDP}}{\Sigma_{obs}\left(\frac{1}{d_{obs}}\right)^{IDP}}$$

Where:

$B(x,y)$ is the estimated bird density at the prediction point located at coordinates (x,y); *obs* represents the observed points within the 1 × 1 km grid cell; b_{obs} is the observed bird density at each point; d_{obs} is the distance from each observed point to the prediction point (x,y); and *IDP* is the IDW Power, a parameter that determines the influence of distance on the weights assigned to observed points.

For distances between observation and prediction points equal to zero, the IDW algorithm applied an infinite weight, meaning that if the location (x,y) of a prediction coincided with the location of an observation, then prediction density would be identical to the observation density.

Step 4: Generate IDW Predictions. The IDW approach for generating seabird density predictions was implemented using the "Gstat" package (Pebesma & Wesseling, 1998; Pebesma, 2004) in R (R Core Team, 2016). To determine the optimal IDW power for each species and season, we conducted leave-one-out cross validation (LOO-CV) using additional functions within the "Gstat" package.

LOO-CV involved iteratively removing a single prediction location from the IDW algorithm, generating a density estimate for that location using EQN1, and comparing it with the withheld data. This process was repeated for each location with observations, and the error was calculated as the difference between the prediction and the withheld data. The root mean squared error was then calculated using these errors.

We used LOO-CV to tune the IDW power parameter separately for each season and bird species. Optimal IDW powers were determined using a Limited Memory Broyden-Fletcher-Goldfarb-Shanno optimization algorithm, implemented by the "stats" package in R. Limited Memory Broyden-Fletcher-Goldfarb-Shanno optimization involved bounding constraints; in our case, we constrained the IDW power to be between 1 and 3. The optimal power for each season and species was defined as the power that minimized the root mean squared error calculated through LOO-CV.

Step 5: Finalize Seabird Density Predictions and Optimization. Once the optimal IDW power was determined, final seabird density predictions were made on the 5′ × 5′ seabird prediction grid. Although we explored other tuning parameters, such as max distance and max points, these parameters did not meaningfully improve model fit and were not included in the IDW expression provided earlier.

Component III: Converting 2D Densities to 3D

The final component (3D assessment) provides species-specific estimates of seabird density at heights at least 10 m ASL. This 3D conversion integrated three sets of information: (1) response curves (logistic regressions) for each FG that describe the log odds of a binary behavior: the predicted probability of flying higher than versus lower than 10 m based on wind speed (Component I); (2) the 2D density estimates for 44 species (Component II); and (3) the probability of a seabird species flying above 10 m given the windscape for a specific 5′ × 5′ grid cell (Component III).

Supporting Data

Windscape. The windscape analysis (i.e., the strength of winds by location) used data from the CA-20 and Northwest Pacific

modeled wind-speed assessment provided by NREL (2023). Both annual and seasonal averages were determined. The raw data encompassed a 20-year period (2000–2019) and had a temporal resolution of 5-minute time steps. These data were down-sampled to derive a 15-minute time step to balance increased granularity with practical considerations such as data volume, computational burden, statistical robustness, and resource allocation. For the purposes of this study, a 15-minute interval provided sufficient resolution to capture meaningful variation in wind speed while maintaining manageable data complexity and resources for integration into the 3D Framework. The raw data also had a spatial resolution of 2 × 2 km and were trimmed to match the extent of the seabird prediction domain.

The 2D density estimates were converted into 3D densities with flight height in three steps:

Step 1: Quantifying the Windscape

For each grid cell having a 2D density prediction, the high-resolution wind speed measures were grouped into bins of 0.5 m/s covering the full range of wind speeds that are typically observed at 10 m ASL, from 0 to > 30 m/s. These were tallied to generate a histogram of the frequency of all observed wind speeds encompassed by the data.

Step 2: Calculate the Probability of Each Species Flying Over 10 m

The probability of a given species flying to exceed 10 m in each season per grid cell:

$$FPA(S,FG,GC) = \sum_{ws(GC)} P(ws,S) * FP(ws,FG) \text{ (EQN 2)}$$

Where:

FPA is the overall average probability of a seabird species flying > 10 m (unitless); S is the season; FG is the flight-style grouping that the species belongs to; GC is the grid cell (native to the 2D density estimate); WS is the wind speed bin (in 0.5 m/s intervals); P is the probability of being in a specific wind speed bin (i.e., the count of timesteps in bin/total count of timesteps; unitless); and FP is the probability of a seabird flying > 10 m, as estimated by the logistic regression model in Component I for a given wind speed and flight group (unitless).

Step 3: Calculate the Seasonal Density of Each Seabird Species at Heights 10 m ASL

Part A: Seasonal Estimates. With these season- and FG-specific estimated probabilities of flying above 10 m, the density of each seabird species exceeding 10 m could be calculated using the 2D density estimates:

$$SA10(S,SB,GC) = SA(S,SB,GC) * FPA(S,FG,GC) \text{ (EQN 3)}$$

Where:

SA10 is the seabird density > 10 m ASL (number of seabirds/km^2); SB is the seabird species; and SA is the seabird density (count/km^2); and the remaining components of the formula have been defined under EQN 2.

Step 3 can be described as a numerical integration of the wind speed distribution with respect to the FG-specific flight height as a function of wind speed (Component I). This process estimates the overall probability of exceeding 10 m given the distribution of all observed wind speeds.

This framework and method (Part A) have been graphically represented in Fig. 7. This figure shows the estimation of density of Sooty Shearwater *Ardenna grisea* above 10 m in the Humboldt WEA. Because of their responsiveness to the wind and their significant contribution to the overall CCS seabird community, Sooty Shearwaters were one of the species warranting a more detailed evaluation with the 3D Framework. The probability curve representing the propensity of Sooty Shearwaters to fly at altitudes overlapping RSZs (see Fig. 8, right panel of Fig. 7) indicates that all individuals exposed to winds of 18–27 m/s (i.e., 40–60 mph) will likely be maneuvering above 10 m ASL 50%–85% of the time. However, even in the wind-rich Humboldt WEA, winds > 18 m/s have been and are expected to remain episodic (Fig. 7, left panel; also see Fig. 11 for an alternative presentation of Humboldt WEA wind speed data). Therefore, the annual predicted average density of Sooty Shearwater flying above 10 m is 0.48 birds/km^2.

Part B: Annual Estimates. The annual estimates of seabirds flying above 10 m were calculated by combining seasonal estimates.

$$SA10(SB,GC) = \sum_{S} PS(S) * SA10(S,SB,GC) \text{ (EQN 4)}$$

Where:

PS is the probability of being in a specific season; and the remaining components of the formula have been defined under EQN 2.

RESULTS

We begin by presenting the flight height and wind speed probability curves for each of the 18 FGs included in the 3D Framework (Component I; Fig. 8), which are fundamental for increasing the dimensionality of predictions from 2D to 3D (Components II and III). We then shift focus to the substantial proportion of the CCS seabird community included in the 3D Framework (Fig. 9; Appendix A, Table A2; Appendix B) by presenting intermediate results and ultimate outcomes of Components II and III in the following order:

- Windscape results relevant to converting 2D predictions to 3D (Figs. 10–11);
- Aggregate community predictions in both 2D and 3D (Figs. 12–13);
- Four case studies (Figs. 14–18) spotlighting two species that together constitute ~50% of CA's seabird population, Sooty Shearwater and Common Murre *Uria aalge,* as well as two species of conservation interest: Marbled Murrelet *Brachyramphus marmoratus* (Federally threatened, CA Endangered) and the Ashy Storm Petrel *Hydrobates homochroa* (CA Species of Special Concern);
- Annual density prediction maps for all 44 taxa included in the 3D Framework (Appendix B);
- Seasonal density prediction maps for a subset of migratory species that move in and out of the CCS during the year (Appendix C);

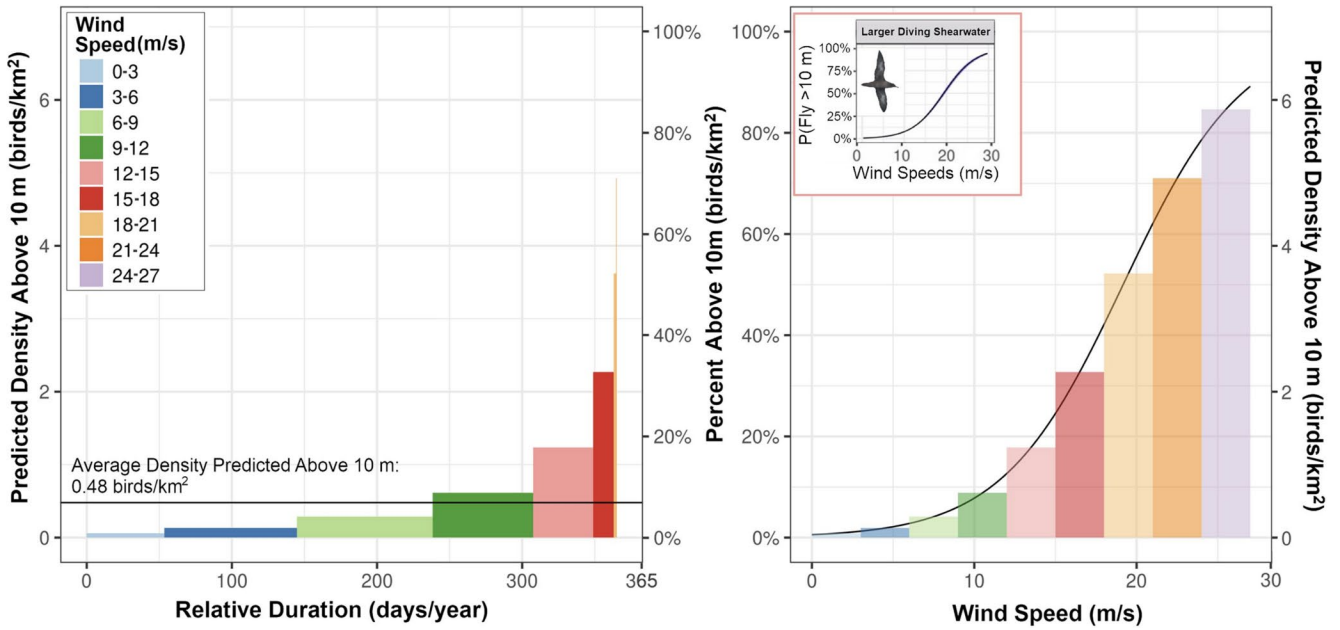

Fig. 7. Visual representation of 3D Seabird Framework for Sooty Shearwater *Ardenna grisea* in the Humboldt Wind Energy Areas. The results of the framework analysis are provided at a resolution of wind speed categories of 3 m/s. While, in practice, this analysis is conducted for each season, in this depiction the seasons were combined to provide an annual representation. Left side panel: The relative duration (as width) of each wind speed (denoted by color), and the predicted density and percent of birds estimated above 10 m for each wind speed, is provided. By considering both the frequency of these wind speed conditions and the density of birds in each condition, the average density of birds can be estimated given the windscape in the area. This is visually represented as the height of these bars, indicating the average density of birds over 10 m considering the wind distribution and flight behaviors. Bar widths are based on the prevalence of windspeeds within the 20-year record. Right side panel: The results of the logistic flight height regression for the predicted density and percent above 10 m for Sooty Shearwater by wind speed category, color-coded to match the left panel.

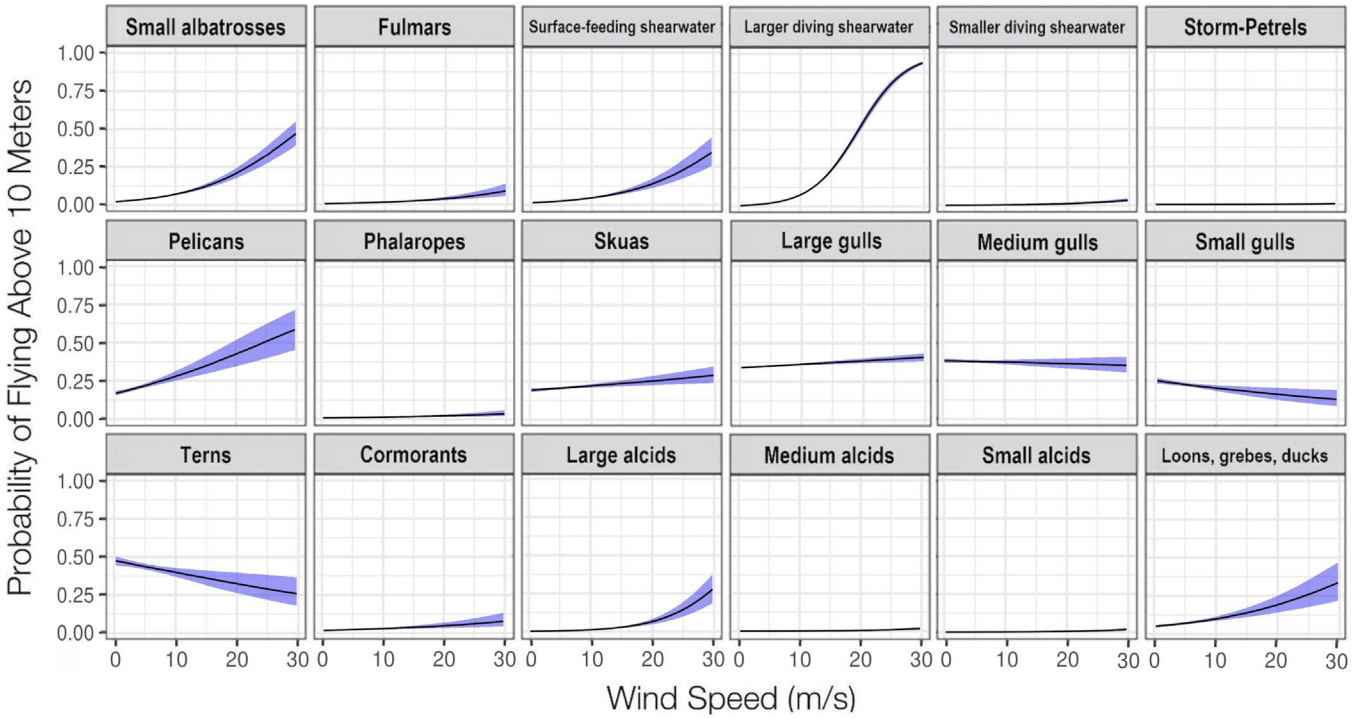

Fig. 8. Probability of flying at least 10 m above sea level (ASL) as a function of varying wind speeds (m/s) for each flight-style grouping. Data and predictions encompass the full range of wind speeds needed for turbine rotation (3–25 m/s). Purple shaded regions around each line depict the bootstrapped 95% confidence intervals.

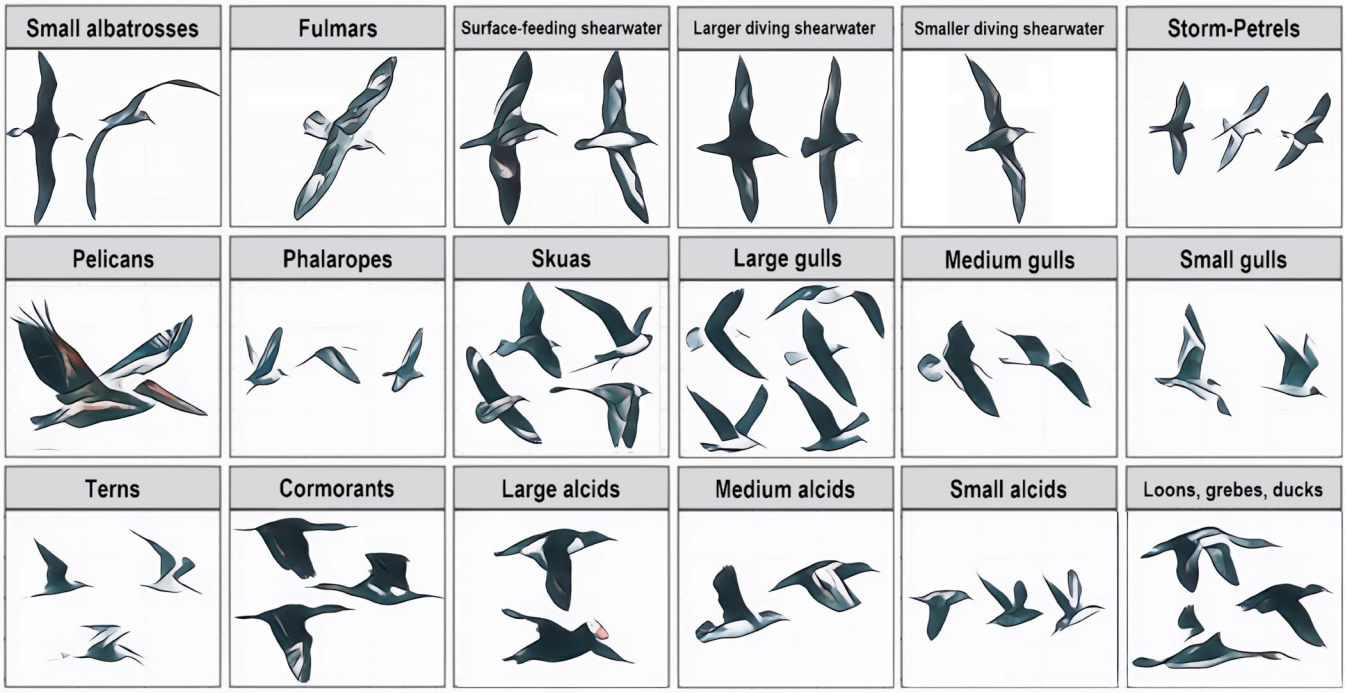

Fig. 9. Seabird types included in the 3D Seabird Collision Vulnerability Framework. Seabirds are organized by flight-style grouping. Note that bird sizes have been adjusted for clarity and ease of comparison of wing and body morphology, rather than representing their actual relative body sizes.

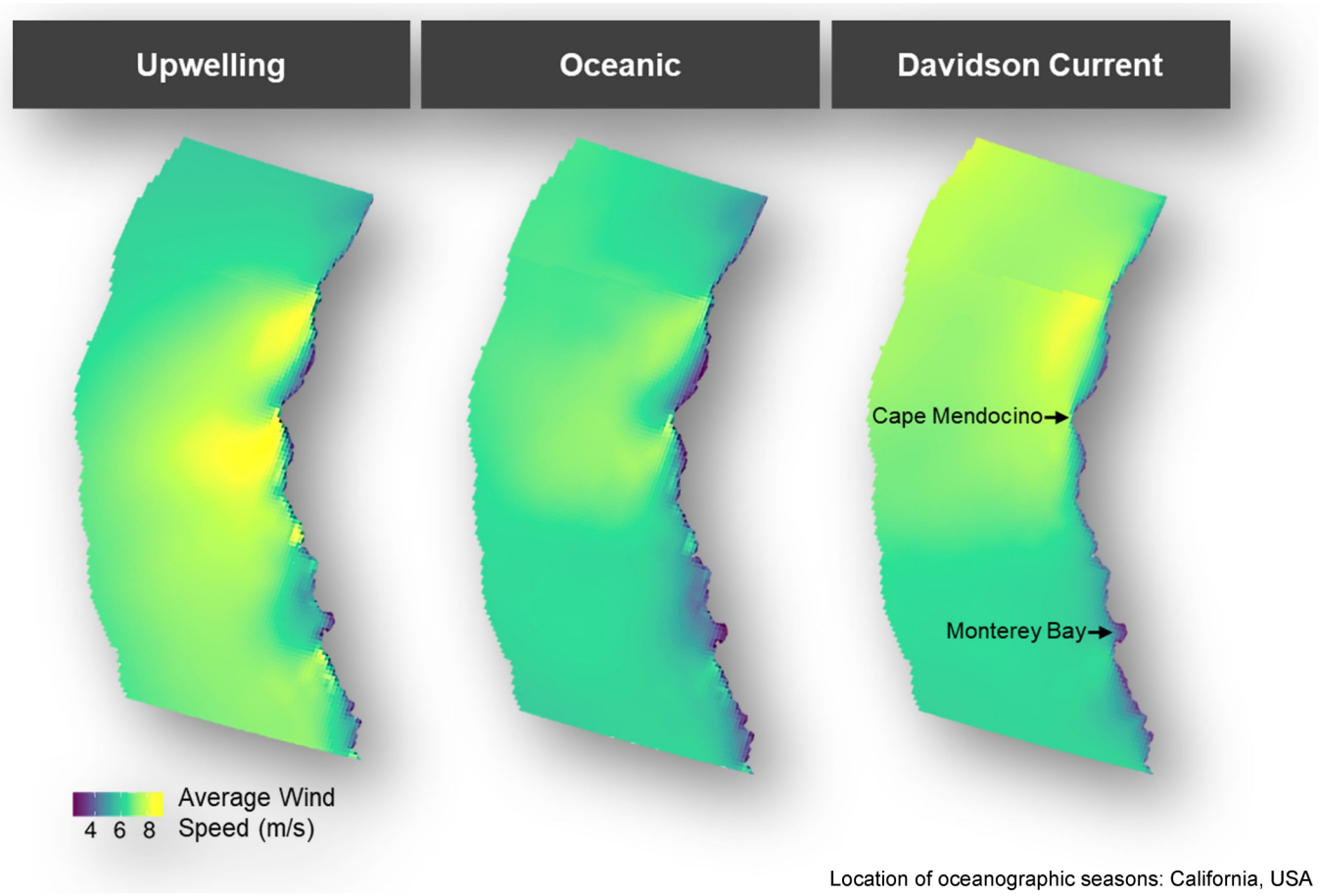

Fig. 10. Offshore windscape for each oceanographic season. The 20-year (2000–2019) wind speed averages (m/s) off California (USA) were derived from CA-20 and Northwest Pacific wind speed models provided by National Renewable Energy Lab. Seasonal averages were calculated based on wind speeds at turbine hub height (150 m above sea level). Data source: National Renewable Energy Lab (2023).

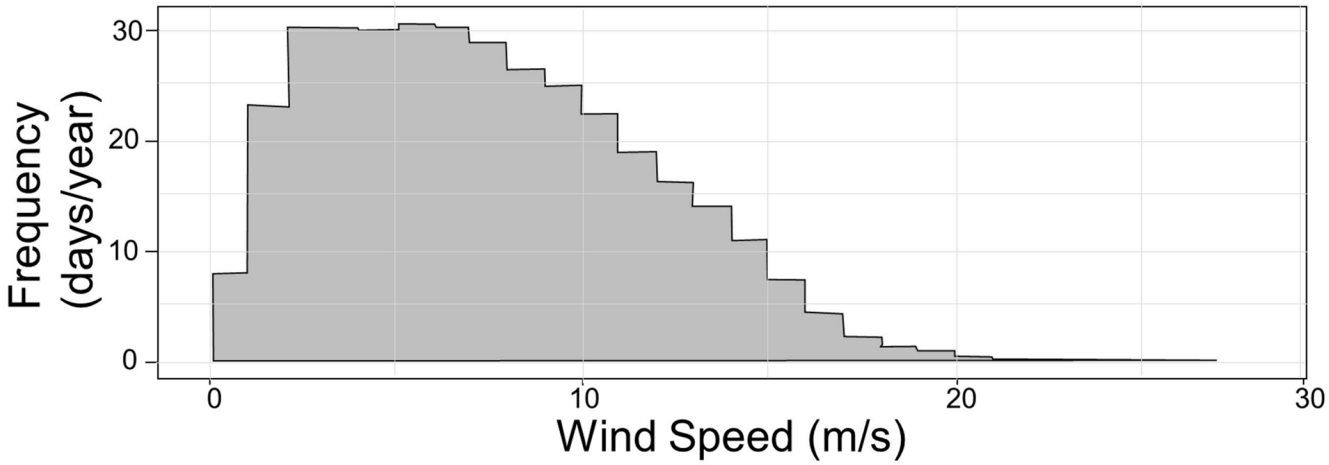

Fig. 11. Annual frequency distribution of wind speeds from the Humboldt Wind Energy Area (WEA). Histogram depicting the annual frequency distribution of all wind speeds estimated at the center point of the Humboldt WEA (USA). Data sourced from CA-20 wind speed data provided by the National Renewable Energy Lab. Wind speeds were averaged at turbine hub height (150 m above sea level) into 15-min intervals and binned into 0.5 m/s intervals for frequency analysis. Data source: National Renewable Energy Lab (2023).

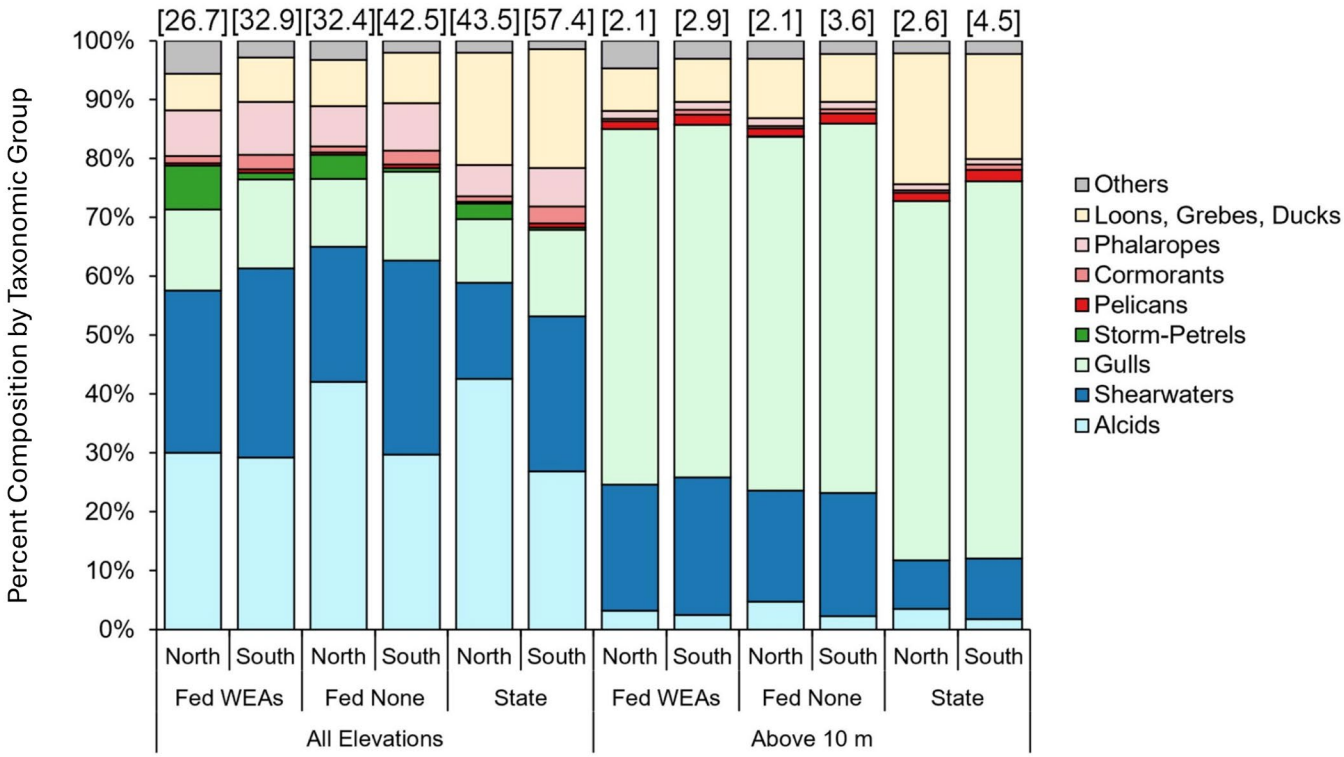

Fig. 12. Comparing 2D and 3D predictions of California (USA) Current seabird community composition across geographic regions. To assess differences in the composition of California's seabird community from 2D (all elevations) and 3D (> 10 m above sea level) perspectives, the study area was divided into six regions. Cape Mendocino (40.44°N) served as the boundary between north and south areas, and east-west divisions were determined by distance from the coastline, resulting two main categories: "State," representing waters under state jurisdiction that extend out to 4.8 kilometers (km) (i.e., 3 miles [mi]); and "Fed," representing waters beyond this limit. Within "Fed" waters, two additional subdivisions were made: "None" for areas not currently considered for wind energy development (4.8 to 32 km [3 to 20 mi] offshore), and wind energy areas (WEAs) representing the western extent of waters off California physically capable of supporting offshore wind mooring infrastructure (i.e., shallower than 1,300 m; 32 to 80 km [20 to 50 mi] offshore) and inclusive of all currently leased WEAs. No WEAs are proposed south of Point Conception. Taxa were grouped broadly for clarity, with average annual density estimates (birds/km^2) provided above each column.

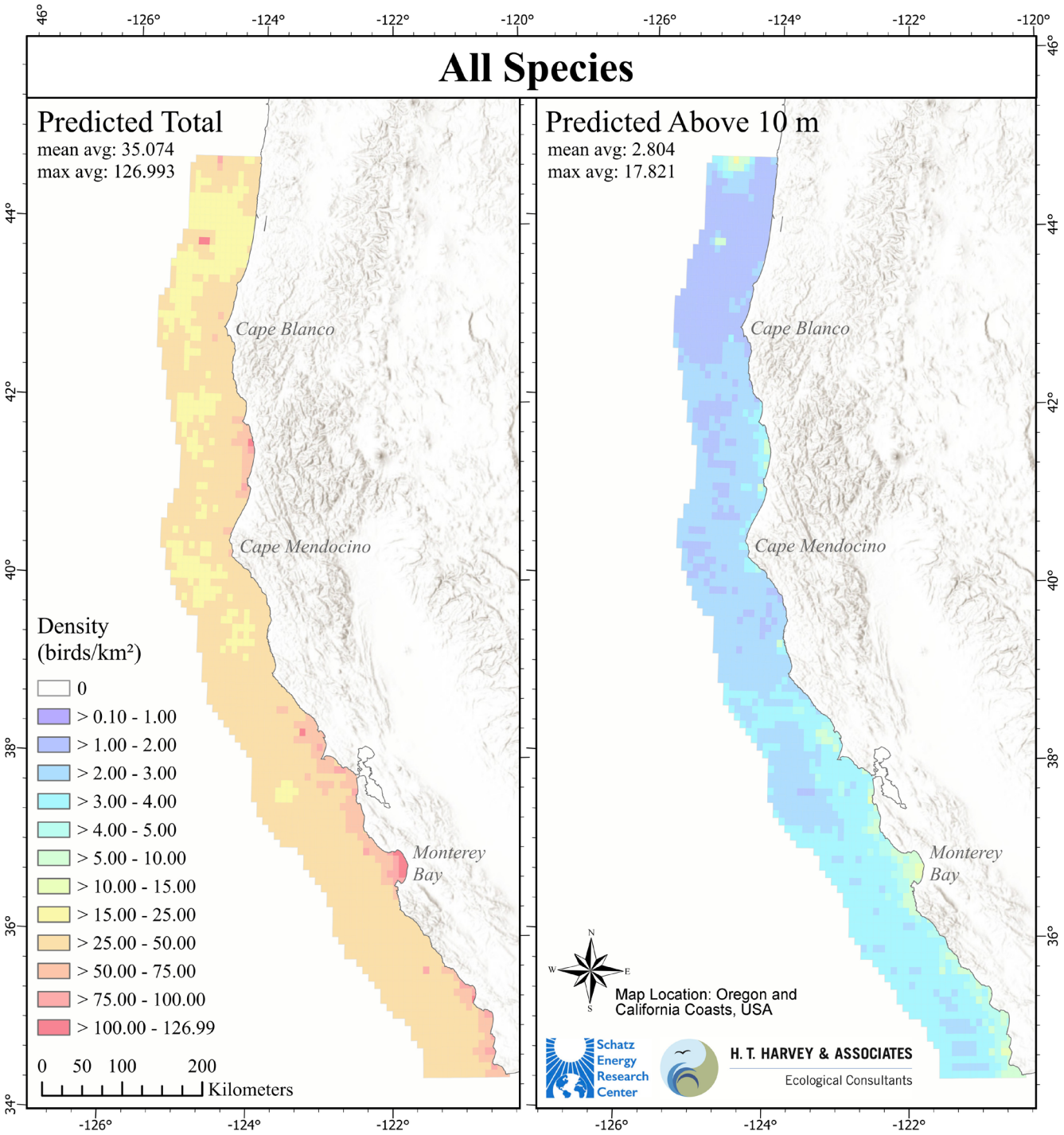

Fig. 13. Annual 2D and 3D predictions for California (USA) Current seabird community. Predicted densities for all 44 seabird taxa included in the 3D Framework from a 2D perspective of the total community (left), as well as a 3D perspective of individuals flying at least 10 m above the sea surface (right). The mean average and maximum average values, shown at the top of the panels, are measured in birds/km^2. These values represent the average expected density across all cells and the highest density predicted within a single cell in the area, respectively.

- Prediction quality metrics, determined through LOO-CV, for each species and season summarized in both tabular (Appendix D, Table D1) and visual (Appendix D) formats;

- Fundamental background information on the ecology, morphology, and flight behavior of seabirds included in the 3D Framework (Appendix E).

Flying at Collision Risk Height

A mixed-effects logistic regression model was fitted to 74,802 observations across 18 FGs (Appendix A, Table A4) to predict the probability of seabirds flying > 10 m and thus overlapping RSZs (Fig. 8). Across all observations, the likelihood of a bird flying > 10 m increased by 8% for every 1 m/s increase in

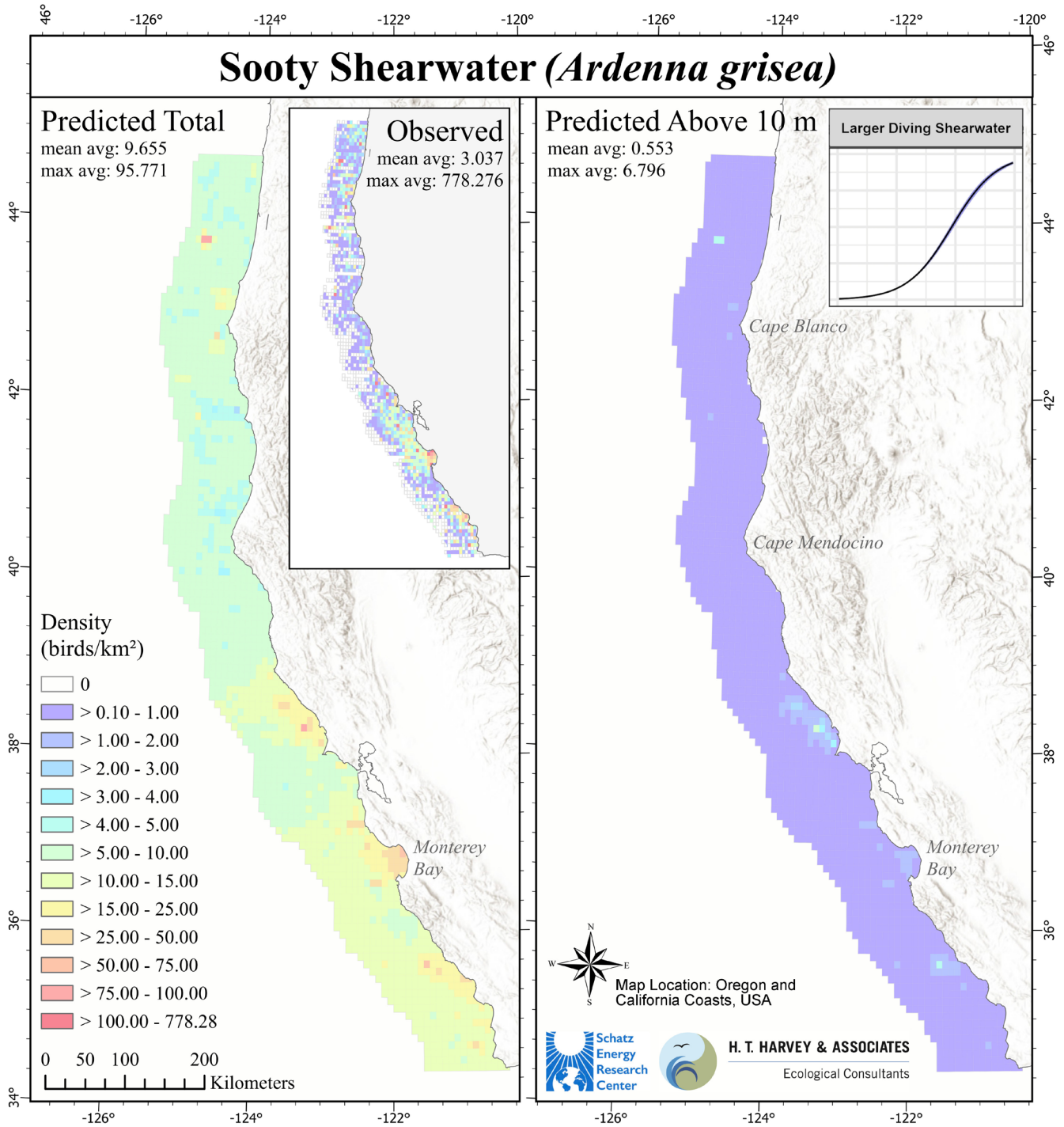

Fig. 14. Annual 2D and 3D predictions for Sooty Shearwater *Ardenna grisea*. An abundant and widespread species likely to fly at rotor swept heights.

wind speed (logistic regression, $p < .001$, $df = 76{,}367$). However, when examined by FG, seabird responses to increasing wind speed were variable (Fig. 8): birds in some FGs were more likely to fly at higher altitudes, whereas those in others were less likely to do so; some FGs were unaffected by wind speed or exhibited lower flight heights at higher wind speeds.

Several FGs exhibited distinct responses. Large diving shearwaters, owing to their morphology and flight style, showed a pronounced response to wind, with both flight height and chance of entering the RSZ increasing steeply with wind speed (Appendix E). Small albatross and surface-feeding shearwaters showed similar patterns, although to a lesser extent, requiring stronger winds to reach comparable heights. Pelicans also showed increasing flight height with wind speed, despite not flying by dynamic soaring. In contrast, storm petrels, phalaropes, cormorants, and alcids exhibited minimal probability of flying > 10 m ASL regardless of wind speed; these groups rely

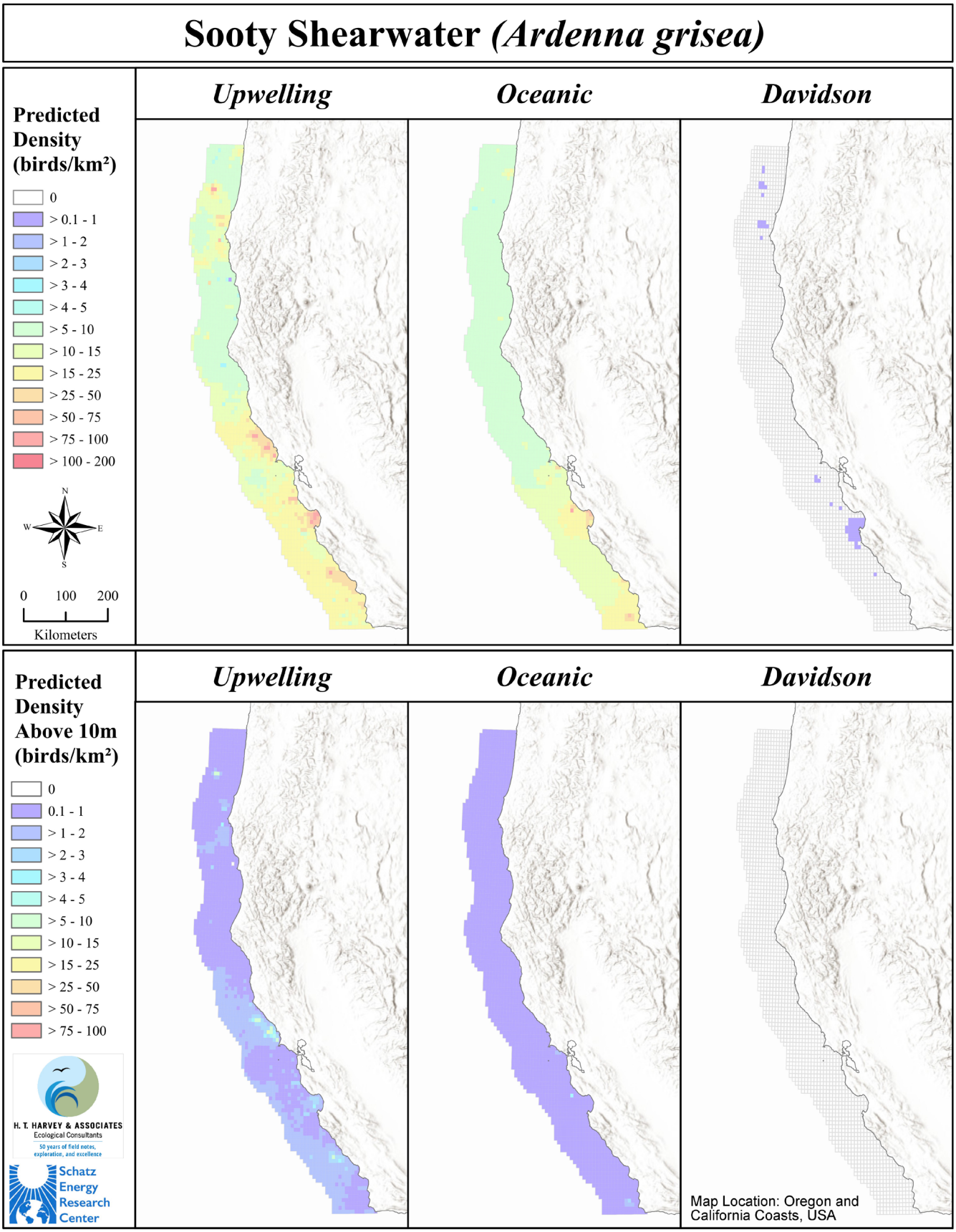

Fig. 15. Seasonal 2D and 3D predictions for Sooty Shearwater *Ardenna grisea*. The cells lacking color in the Davidson Current season result from an absence of this species during that time, as individuals are nesting in the southern hemisphere.

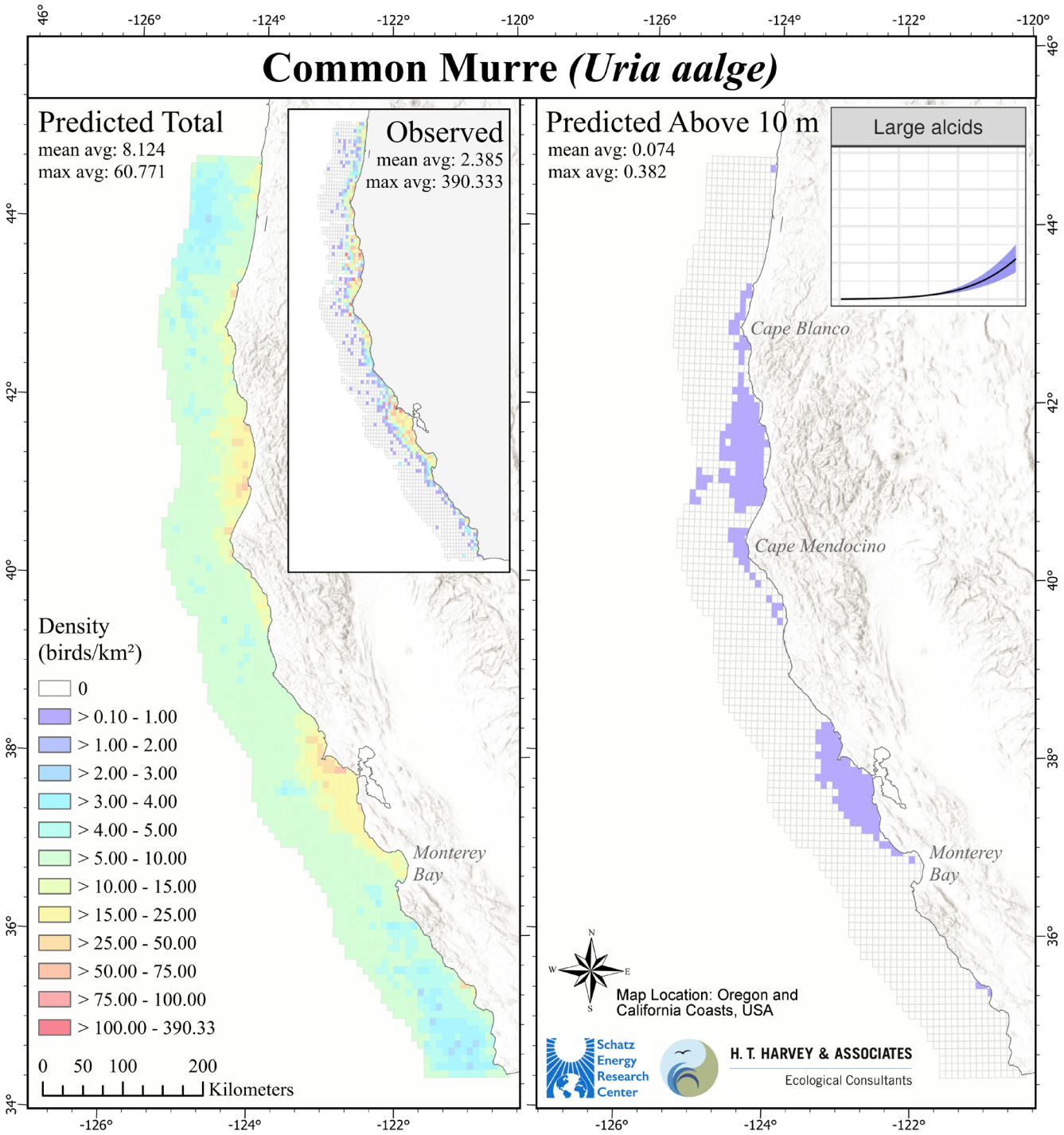

Fig. 16. Annual 2D and 3D predictions for Common Murre *Uria aalge*. An abundant and widespread species with a relatively low probability of flying at rotor swept heights.

primarily on flapping or flap-gliding flight, for which wind can be somewhat of an impediment (Appendix E). Finally, certain FGs, such as medium gulls, small gulls, and terns show a decline in the probability of entering the RSZ as wind speed increases. Flying closer to the surface in strong winds reduces drag. The exact coefficients associated with the FG-specific flight height regressions presented here (Fig. 8) are available in Appendix A, Table A4.

Seabirds in 3D

Species Included

The seabird community included in Components II and III (Fig. 9) represents a diverse array of the CCS's abundant seabirds. Among the 109 taxa present in the database supporting Component II, 44 met the criterion of being observed within at

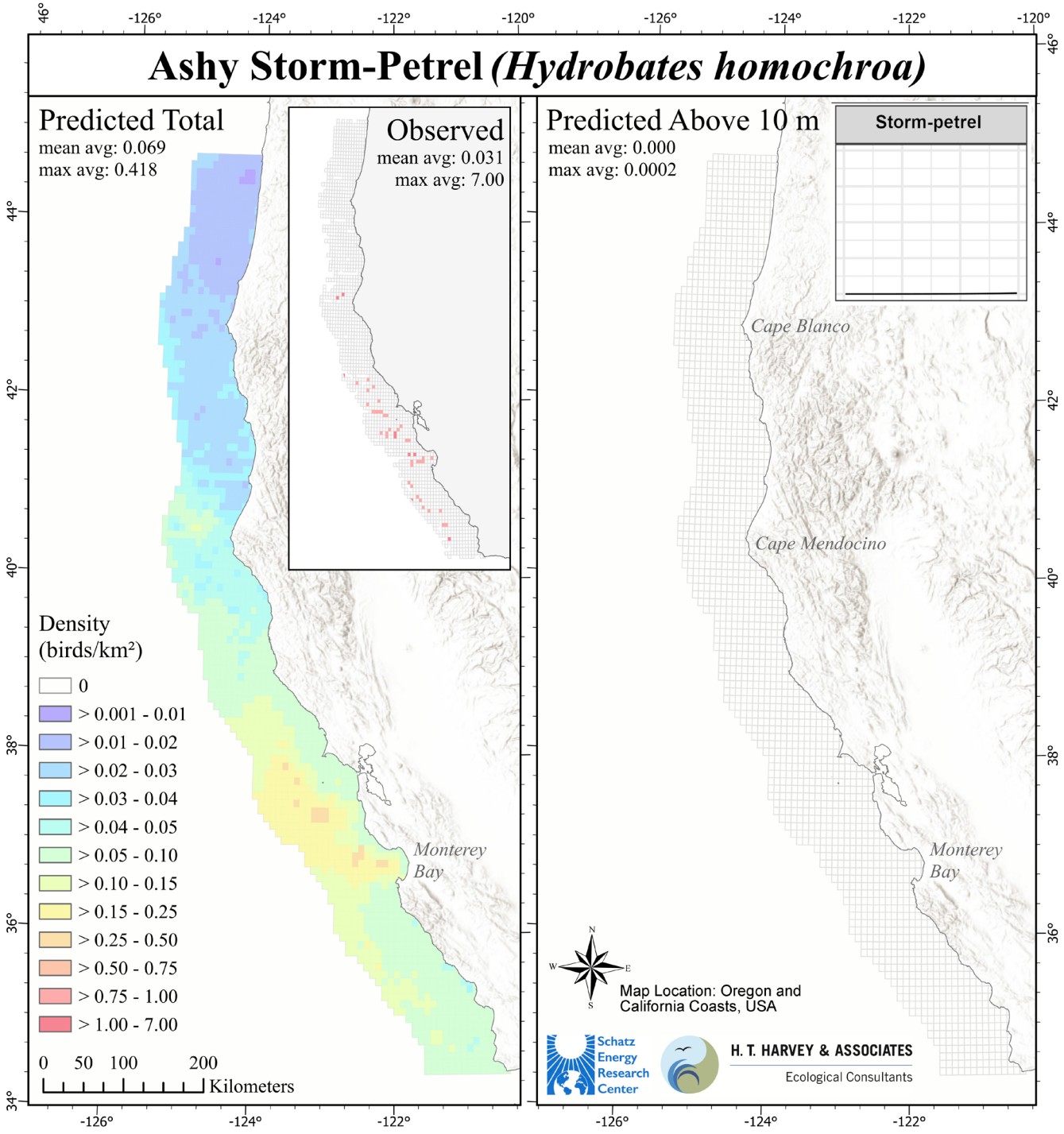

Fig. 17. Annual 2D and 3D predictions for Ashy Storm Petrel *Hydrobates homochroa*. A special status and range-restricted species unlikely to fly at rotor swept heights.

least 100 km^2 of survey effort. These taxa include both highly abundant species, such as the Sooty Shearwater and Common Murre, collectively constituting over 50% of individuals counted at-sea, as well as relatively rare (though locally abundant) members such as special status Marbled and *Synthliboramphus* murrelets. There are other endangered/threatened seabird species that occur within the CCS, especially the OCS, but not in numbers sufficient for our analysis, e.g., Hawaiian Petrel *Pterodroma sandwichensis* (flight characteristics similar to large diving shearwaters).

At-sea counts of the 44 included taxa revealed notable patterns. First, Sooty Shearwater and Common Murre accounted for 55.7% of the total count. Otherwise, 13 of the 44 taxa accounted for ~90% of the total individuals, 17 of 44 accounted for > 95%, and 27 of 44 species accounted for > 99% of the community (see Appendix A, Table A2).

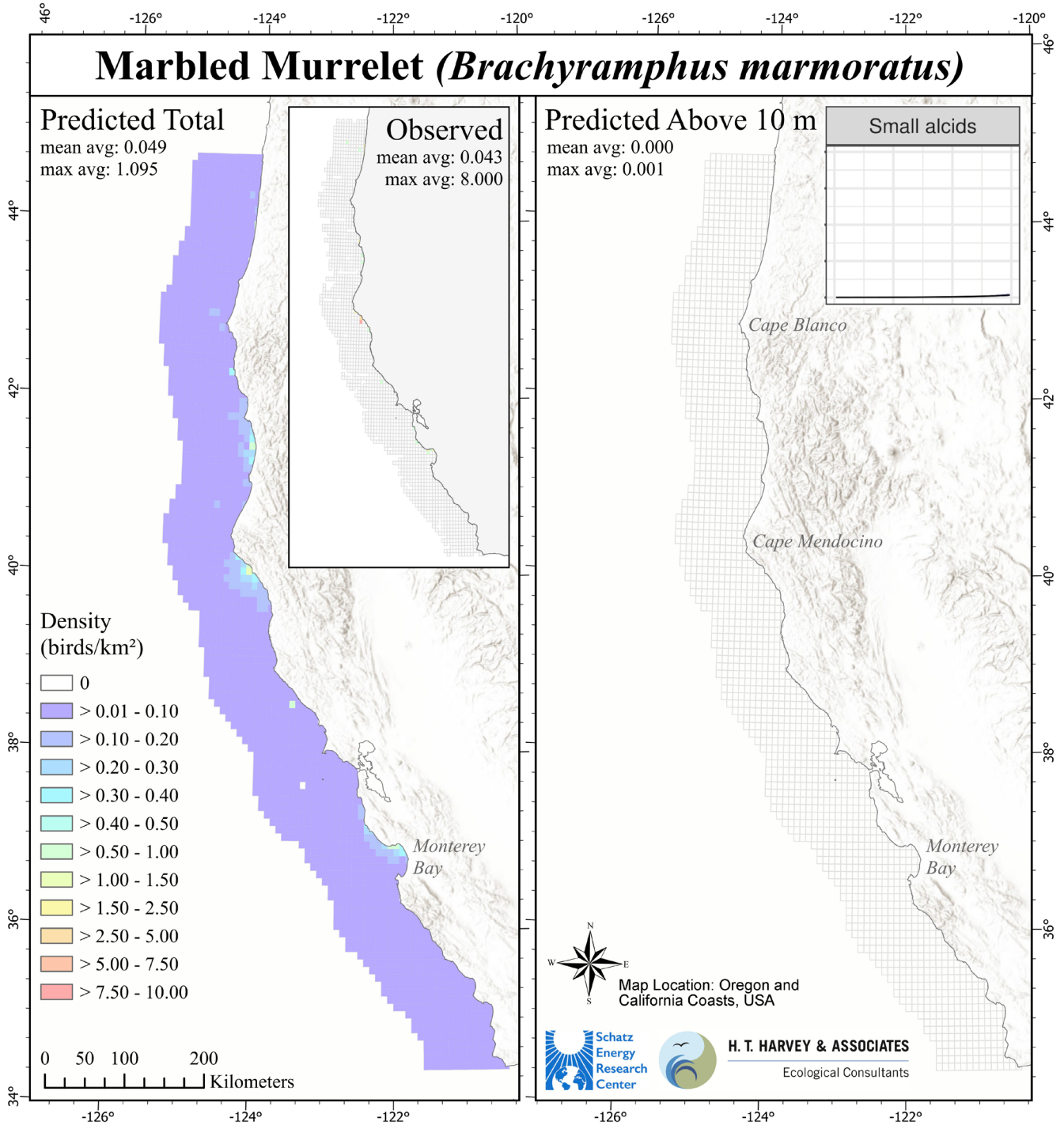

Fig. 18. Annual 2D and 3D predictions for Marbled Murrelet *Brachyramphus marmoratus*. A special status and extremely coastal species unlikely to fly at rotor swept heights.

Although most density predictions were species-specific, three of the 44 taxa were grouped due to challenges in distinguishing sympatric species during aerial surveys: Red and Red-Necked phalaropes *Phalaropus* spp.; Western and Clark's grebes Aechmophorus spp.; and Scripps's, Guadalupe, and Xantus's murrelets *Synthliboramphus* spp.

An additional 65 species were observed within waters of the CCS but too infrequently to be included (Appendix A, Table A3). One species, Cook's Petrel *Pterodroma cookii*, technically met the inclusion criteria but was recorded in only 17 km^2 more than the 100 km^2 threshold, and its rarity resulted in predictions that did not meaningfully influence community-level predictions. Other notable species excluded due to rarity were Hawaiian Petrel (gadfly petrel) and Short-tailed Albatross *Phoebastria albatrus* (small albatross), both federally listed as endangered and species of conservation concern. All three of these dynamic soaring species

have been increasing in the CCS during recent decades, a result of conservation measures at their distant breeding sites, and may therefore meet inclusion criteria in future analyses.

Converting 2D to 3D

Seasonal Windscape Off CA. The CCS seasonal windscape exhibits distinctive variations across the three oceanographic seasons (Fig. 10). During the Upwelling period, a prominent wind-driven feature of the CCS, winds are persistently strongest, predominantly from the northwest. These winds are strongest near the coast, especially around capes and headlands. In contrast, the Davidson Current season is characterized by lower average wind speeds that are not uniform across the offshore region; winds are perceptibly stronger in offshore and in northern portions of the study area. Seasonal differences in the windscape have important implications for some seabird FGs, particularly with respect to the probability of birds flying > 10 m ASL. In addition to these seasonal patterns, longer-term changes in species composition and abundance in the CCS, as noted above, may also influence the collective vulnerability of the seabird community. Although long-term average wind speeds offer valuable insights into spatial and temporal patterns within the windscape, seabird flight heights can vary in response to site-specific wind conditions (Ainley et al., 2015; Spear & Ainley, 1997a, 1997b).

Moreover, during the Upwelling season, strong winds come in several-day-long pulses, 12–15 m/s or higher, interspersed with periods of calm. Pulsed, rather than persistent, winds are most conducive to increased ocean productivity. For instance, in the Humboldt WEA, although maximum wind speeds typically remain < 20 m/s for most days of the year, there are recurring periods during the Upwelling season and during the winter Davidson Current season when wind pulses greatly exceed this threshold (Fig. 11). During these episodes of particularly strong winds, dynamic soarers, like large diving shearwaters and small albatross, regularly reach heights exceeding 10 m ASL, as they also do at 12–15 m/s. Although extreme wind events (> 20 m/s) are rare in any given year (Fig. 11), they represent critical periods when seabirds in specific FGs (e.g., large diving shearwater, pelicans) are likely to fly at heights facilitating overlap with RSZs.

Community-Level Predictions

The composition (Fig. 12) and density (Fig. 13) of the CCS seabird community exhibits broad-scale patterns of variability north to south, and east to west, showing different species composition > 10 m ASL relative to the overall community, and across seasons. The predictions generated by the 3D Framework enable a range of spatial and temporal analysis of the CCS seabird community; a few are briefly explored in the following sections.

Differences in Composition. When considered in aggregate, the composition of the seabird community varied most notably in the vertical dimension (Fig. 12). Some dominant seabird types, when evaluated from a 2D perspective, constituted only a small portion of the community > 10 m ASL (e.g., few alcids flew at that height), whereas the dominance of gulls above this threshold was much greater than calculated in 2D analysis. Above 10 m, the seabird community across all regions was primarily composed of gulls and shearwaters, collectively accounting for at least 80% of the individuals, with a diverse collection of other FGs forming the remainder of the community. Gulls, which are fairly abundant, fly higher ASL and show limited response to wind speed (Fig. 8). In contrast, shearwaters are responsive to wind speed and are far more abundant than any other dynamic soaring species (e.g., small albatross).

All six geographic regions considered were dominated by alcids (primarily Common Murre) and, collectively, just three groups—alcids, shearwaters, and gulls—accounted for 70% or more of individuals present (Fig. 12). The remaining ~30% of individuals in the community showed the following variations by region: a greater proportion of alcids north of Cape Mendocino and within 32 km (20 mi) of the coast, a robust presence of storm petrels offshore north of Cape Mendocino, and a concentration of loons, grebes, and ducks in state waters (0 to 5 km from the coast).

Differences in Density. The predicted densities of all 44 seabird taxa annually averaged 35 birds/km^2, with a maximum site-specific average density of 127 birds/km^2 (Fig. 13). However, when considering birds flying at least 10 m ASL, the predicted densities were lower, averaging 2.8 birds/km^2 with the maximum site-specific average density prediction equaling 17.8 birds/km^2 (Fig. 13). Two broad, region-wide patterns were evident from the density distribution maps for all species: (1) densities were greatest in waters over the inner shelf and decreased as distance from shore increased (including many locally breeding species), and (2) densities were greater in the southern portion of the study area and tapered off with increasing latitude (Fig. 13). Notable concentrations of seabirds were found in association with inner shelf areas from Point Conception, extending north beyond Morro Bay, as well as Monterey Bay extending north to encompass the Gulf of the Farallones (Fig. 13).

It is crucial to provide context for the instantaneous 2D and 3D density estimates presented for the overall seabird community, as well as for each individual species discussed in subsequent sections of this report. These values offer estimates of bird densities at any given point in time, denoted as "birds/km^2" but without a temporal component. Derived from data spanning several decades, these "collision vulnerability estimates" provide instantaneous expectations of seabird densities at and below RSZs as a function of these multi-decadal seasonal and annual conditions. For instance, an average density of 35 birds/km^2 for all seabirds included in the 3D Framework across the entire prediction region can be interpreted as follows: on average, approximately 35 birds (or a similar order-of-magnitude density) could be expected to be present within each square kilometer across the entirety of the prediction area at any given moment throughout the year (or season when considering seasonal predictions), assuming wind speed and bird densities similar to long-term historical conditions.

The instantaneous collision-vulnerability estimates presented herein offer several advantages. First, they are derived from comprehensive data spanning multiple decades, providing a more representative range of environmental conditions and extremes than approaches focused on higher-resolution temporal variability could capture. By incorporating data from various periods, including multi-decadal extremities, these estimates offer a robust representation of long-term historical averages. Second, these estimates provide an order-of-magnitude expectation of bird presence within a given area, considering bird distributions across different heights that may expose them to RSZs. This nuanced understanding enhances our

comprehension of seabird abundance and distribution, particularly in areas of potential collision risk. Third, they serve as a valuable tool for comparative analysis across groupings such as species, sites, and vertical strata. This facilitates assessments of region-wide collision vulnerability and supports targeted conservation efforts.
Although these instantaneous collision vulnerability estimates offer clear benefits, it is also important to recognize their limitations. Despite being based on long-term averages, they do not capture rapid or temporally sensitive changes resulting from single events or anomalous conditions that may impact the seabird community. Consequently, they may not accurately reflect short-term fluctuations, such as those leading to "mortality events" due to wind turbine collisions.

It is essential to acknowledge that these instantaneous density estimates primarily reflect the community-level vulnerability to collision with RSZs by providing a metric similar to seabird passage rates at RSZ heights. An important distinction between the instantaneous vulnerability estimates quantified here and the passage rates input into collision risk models to generate collision rates is that passage rates (and the resulting collision rates) incorporate an explicit temporal component, expressed in units of birds/km^2/yr. It is important to note when interpreting the instantaneous vulnerability metrics that, while passage rates and collision rates are related, they are not directly equivalent. Actualized collision between seabirds and RSZs will be influenced by a multitude of factors beyond vulnerability and passage rates (e.g., bird behaviors that affect their ability to detect and avoid rotor swept zones at macro-, meso-, and micro- scales). Therefore, while the instantaneous 2D and 3D density estimates presented throughout this report offer insights into seabird distributions and potential vulnerability to collision risk, they should be interpreted mindfully and in conjunction with other relevant metrics and considerations.

Species-Level Predictions

Map Overview. Graphical representation of various 2D and 3D species-level density predictions for the 44 included seabird types have been generated, both annually and by season. The following summary is organized to aid in the interpretation of these species-specific maps, with details presented first for all 2D and 3D maps, followed by information specific to annual maps, and finally details specific to seasonal maps.

We illustrated these points, relevant to all density maps, by reviewing a few species, following this summary:

- Prior to examining the details of the 2D and 3D prediction maps, we advise reviewing the guidance provided in the Community-Level Predictions section for interpreting the density estimates. Although this guidance was tailored for the All Species map (Fig. 13), it is equally applicable for interpreting the species-level prediction maps.

- 3D predictions of bird densities > 10 m can never exceed those of the corresponding overall 2D bird-density predictions, as the birds at > 10 m are inherently a subset of the overall population. Typically, densities predicted at > 10 m are an order of magnitude lower than overall densities due to most of the broader seabird community concentrating their activity in the lowest 10 m ASL (Schneider et al., 2024).

Any grid cells visibly outlined on these maps, but lacking fill color, represent observations and/or predictions that were either equal to zero or extremely small.

Information specific to annual density maps:

- These maps have two panels and four main pieces of information:
  - Predicted Total (left main panel) displays the annual 2D density predictions generated using a spatial interpolation approach, providing insights into seabird densities across unobserved areas based on adjacent observations from at-sea surveys.
  - Observed (left inset panel) visualizes the underlying at-sea seabird count data. It illustrates cells in which surveys were conducted but no individuals were observed; these are outlined in grey and lacking color.
  - Predicted > 10 m (right main panel) shows the annual 3D-density prediction of birds flying in the rotor swept zone (> 10 m), showcasing a key output of the 3D Framework.

Flight Height Probability Curve (right inset panel), for each species, illustrates the relationship between the probability of flying > 10 m and wind speed.

- Mean average and maximum average densities (birds/km^2) are displayed at the top of each main panel. These values represent the average expected density across all cells and the highest density predicted within a single cell in the area, respectively. Further exploration of these metrics is conducted within the context of the four species-specific case studies featured in the Differences Across Species section.

Information specific to seasonal density maps:

- Seasonal predictions were generated for all 44 included seabird species.

- Given the seasonal variability in distribution and density observed in many seabird populations, efforts were concentrated on illustrating this variation for 15 migratory species that reside elsewhere for a portion of the year.

- Each seasonal prediction map for a migratory species consists of six panels:
  - Three columns, dedicated to specific seasons—Upwelling, Oceanic, and Davidson Current.
  - Two rows, representing 2D and 3D predictions, respectively.

Sooty Shearwater. Sooty Shearwaters, for as long as survey data have been available, have been the most widely observed and numerous seabirds in the CCS, despite documented population decreases in recent decades (Ainley & Hyrenbach, 2010; Veit et al., 1997). Although they are a migratory species nesting in the Southern Hemisphere, they are present in the CCS mainly during Upwelling season (decreasing south in Oceanic season). The greatest 2D densities of Sooty Shearwater were observed in Monterey Bay,

with the observed maximum average density reaching 778 birds/km^2 (Fig. 14, left panels). Notably, the observed maximum annual average density was 7.1 times greater than the corresponding prediction (778.3 versus 95.7 birds/km^2, respectively; Fig. 14, left panels). Meanwhile, the mean annual average densities showed an opposing pattern, with predictions 2.2 times greater than observations (3.0 versus 9.6 birds/km^2, respectively; Fig. 14, left panels). This discrepancy reflects the species' highly aggregated distribution, driven by extreme flocking behavior. Flocks exceeding 10,000 birds/km^2 were documented on two occasions (1980 and 2002), but smaller flocks were commonly encountered on surveys (see below). Importantly, during at-sea surveys when Sooty Shearwater presence in the CCS is maximal (i.e., during the Upwelling season and, less so, in the Oceanic season; see Fig. 15), Sooty Shearwaters were not detected in 64.6% of the 22,246 km^2 of survey effort, likely due to their flocking (Fig. 14, left inset panel). For the remainder of Sooty Shearwater observations during these two seasons, flock sizes reported across the 22,246 km^2 of survey effort equaled or exceeded 1,000 individuals in 0.02% of cases, 100 individuals in 1.9% of cases, 10 individuals in 9.1% of cases, and one individual in 35.4% of cases. These patterns indicate that predicted mean densities balance the extremes of individual observations, yielding a more accurate representation of the expected density of Sooty Shearwaters across the prediction area over longer time periods (e.g., years) rather than being representative of anomalous and/or more extreme conditions.

The seasonal distribution of Sooty Shearwaters has been visualized (Fig. 15) to show that this species is present during Upwelling and, less so (more to the south) during Oceanic seasons. They are relatively scarce during the Davidson Current season, having returned to the Southern Hemisphere. Note that in all annual and seasonal prediction maps presented here and in Appendices B and C, cells that have been outlined but are lacking color represent observations and/or predictions that are extremely small or equal to zero. As members of the large diving shearwater FG, Sooty Shearwater morphology enables long-distance travel with minimal flapping via dynamic soaring. Consequently, their flight altitude is highly responsive to wind speed; specifically, the probability of flying > 10 m escalates rapidly with increasing wind speeds, especially winds > 15 m/s (Fig. 14, right inset panel), at which point virtually all traveling Sooty Shearwaters reach heights within the RSZs.

Although extremes can be informative, they do not accurately represent the day-to-day expectations of collision vulnerability. A more representative assessment of potential exposure in the Humboldt WEA over longer time scales requires consideration of the full range of bird-density and wind-speed conditions, not just the episodic conditions of strong winds. For this reason, the 3D Framework relies on capturing the conditions over decadal time scales, an approach that is important for proper interpretation of its 3D Framework collision-vulnerability predictions.

Returning to the Humboldt WEA example, the 3D Framework predicted an annual average density of Sooty Shearwaters > 10 m ASL of 0.48 birds/km^2 (Fig. 15, left panel). This metric of vulnerability can be interpreted as follows: given the multi-decadal observations of the 2D densities of Sooty Shearwaters and the 20-year windscape in the Humboldt WEA, an observer would expect to encounter approximately 0.48 birds/km^2 flying at collision-risk risk heights at any given moment. This value is equivalent to ~8% of the Sooty Shearwaters predicted to be present in any 1 km^2 area of the WEA (Fig. 15, left panel). The right panel in Fig. 15 presents the same information as in the left panel, but the widths of the columns in the right panel change based on the relative duration of each wind speed bin in the Humboldt WEA. In this panel, these columns were plotted with a uniform width to improve visualization of density and percentage predictions across all available wind speeds, including those that occur infrequently.

Overall, the long-term prediction indicates a persistent vulnerability of Sooty Shearwaters to collision with RSZs due to their dynamic soaring and tendency to maneuver at heights of RSZs. As noted, wind conditions conducive to maximizing this vulnerability are most prevalent during the Upwelling season (Fig. 9), coinciding with the highest densities of Sooty Shearwaters in the CCS (Fig. 15).

Common Murre. Common Murre is endemic to the CCS and is abundant year-round in CCS continental shelf waters. It nests in colonies on rocky islands and headlands and visits them for most of the year (Ainley & Boekelheide, 1990; Ainley et al., 2021). Compared with Sooty Shearwaters, murres are more concentrated nearshore (apparently forcing the shearwaters farther offshore; Ainley et al., 2005, 2009) but exhibit similar 2D densities (Fig. 16, left panels). However, unlike Sooty Shearwaters, murres observed away from headland nesting sites (where flight heights may reflect breeding-site activity) show a lower probability of flying > 10 m as wind speed increases (Fig. 16, right inset panel). Consequently, the density of murres flying above 10 m is predicted to be substantially lower than that of Sooty Shearwaters (Fig. 16, right main panel). As with Sooty Shearwaters, the observed maximum annual average density of Common Murres was greater than the resulting maximum annual average density predictions (390.3 versus 60.8 birds/km^2, respectively), and the mean annual average densities exhibited the opposite pattern, with predictions exceeding observations (2.4 versus 8.1 birds/km^2, respectively; Fig. 16, left panels). Similar to Sooty Shearwater, this discrepancy reflects flocking behavior, with larger aggregations occasionally recorded within a single km^2; the largest flock observed across the at-sea survey effort was 2010 birds/km^2 in 1982. Importantly, over a longer period, average densities balance these extremes, providing a more representative estimate of expected Common Murres density expected across the prediction area over a long duration of time (i.e., years to decades). Because Common Murres were present year-round in the study area, their distribution and density exhibited only some minor local shifts associated with changes in seasonal energetic demands. They were more concentrated around colonies while nesting and less concentrated during other seasons when regular colony attendance was not required, including periods of flightlessness during post-breeding molt—rather than the pronounced seasonal changes observed in migratory species (e.g., shearwaters, albatross). Unlike Sooty Shearwater, populations of Common Murres in the CCS have been increasing in recent decades, recovering from former decimation (egging, oil spills; Ainley et al., 2021).

Ashy Storm Petrel. Ashy Storm Petrels are endemic to the CCS, nesting on islands and coastal rocks from northern Baja California, Mexico, to northern central California, and are present in the CCS year-round (Ainley et al., 2020). They are most likely to be encountered in waters overlying the outer continental shelf and slope south of Cape Mendocino and visit colonies for several months of the year (Fig. 17, left panels). Ashy Storm Petrels exhibited a 2D density approximately an order of magnitude lower

than that of Sooty Shearwaters and Common Murres, consistent with population estimates (Ford et al., 2021), and were primarily distributed south of Cape Mendocino. With respect to flight altitude, Ashy Storm Petrels tended to fly < 10 m high across all wind speeds, as indicated by the flat probability curve centered near zero for the storm petrel flight height and wind speed regression (Fig. 17, right inset panel). Consequently, the predicted density of Ashy Storm Petrels flying > 10 m was effectively zero (Fig. 17, right main panel). Like the other two species highlighted above, these storm petrels also form flocks (especially during the Oceanic season, i.e., molting flocks), which explains the discrepancies in observed versus predicted maximum densities. However, due to the relatively low density of this species in general, the magnitude of difference in the observed and predicted mean annual average densities (~0.04 birds/km^2 greater for predictions) were relatively small in an absolute sense. Because this species occurs in the study area year-round, exhibiting only minor seasonal shifts in distribution, seasonal density maps are not presented.

Marbled Murrelet. Marbled Murrelets are coastal residents found within a few kilometers of shore and generally occur at low densities across the region (Fig. 18, left panels). Unlike most CCS seabirds, which nest on offshore rocks and islands, Marbled Murrelets nest in old-growth or mature coniferous forests, sometimes at appreciable distances inland (Fig. 18, left panels). Similar to other species discussed here, Marbled Murrelets may gather in waters near the shore, although not as abundantly as the aforementioned species, leading to discrepancies between observed and predicted maximum densities. Due to their generally low density, the differences between observed and predicted mean annual average densities were relatively minor (~0.006 birds/km^2 greater for predictions). During the Upwelling season, they tend to aggregate in coastal areas adjacent to old-growth forests to minimize travel distances to and from nest sites. Their distribution and density show minor local shifts with changing seasons, and as such, seasonal density distributions are not provided.

Similar to Ashy Storm Petrels, Marbled Murrelets tend to fly below 10 m ASL across all wind speeds (Fig. 18, right inset panel), with a negligible predicted probability of flying > 10 m (Fig. 18, right main panel). One caveat is that when murrelets are traveling between inland nest sites and the ocean at dusk and dawn, throughout the Upwelling season, they ascend in the near-shore ocean to the heights of their nest sites (often tens of meters ASL). Upon return to the ocean, they quickly return to sea level soon after crossing the beach (see Fig. 18).

DISCUSSION

The 3D Framework developed for this project is an innovative effort to better understand the vertical airspace used by seabirds. By integrating extensive data on seabird presence, abundance, and flight height in response to wind speed, and the windscape off CA and OR, the 3D Framework offers valuable insights into the distribution and behavior of seabirds in three dimensions within the CCS.

Collision Vulnerability Assessment

The results of this 3D Framework enhance understanding of how seabird distribution may intersect with OSW infrastructure. Previous studies (e.g., Adams et al., 2016; Kelsey et al., 2025; Leirness et al., 2021; Russell et al., 2023) represent significant achievements that enhanced our understanding of the seabird community in the CCS. However, these studies relied on planar predictions, overlooking the interplay between wind speed and flight height, which are crucial for assessing vertical distributions of seabirds and collision vulnerability. The 3D Framework represents an initial attempt to enhance the dimensionality of seabird density predictions to include the vertical component and facilitate a more explicit evaluation of seabird overlap with RSZs. A primary outcome of the presented assessment is that dynamically soaring species are particularly susceptible to overlapping RSZs, highlighting the need to consider them in OSW permitting and consultation processes, at least in the Pacific. None of the dynamic soaring species nest at locations within or adjacent to the CCS, and they are of low abundance in the North Atlantic region (see, for example, Howell & Zufelt, 2019).

The development of 2D seabird density estimates in the 3D Framework involved integrating data from multiple long-term observation databases, derived from aerial and vessel-based surveys, and correcting counts for flux. Additionally, establishing relationships between flight height and wind speed required re-analyzing data from Ainley et al. (2015) to generate probabilities of flying > 10 m ASL. The 3D Framework included 18 distinct FGs and 44 regularly observed species. Results indicate that most of CA's seabird community remains near the sea surface and close to the coastline. While most FGs fly below the RSZ-height, for those that are likely to enter RSZs, the propensity to do so can vary quite considerably. For instance, large diving shearwaters may fly at a collision risk height anywhere from 0% to 100% of the time depending on wind speed. Moreover, for all included seabird taxa, the 3D Framework predicted annual and seasonal density flying below and above 10 m ASL. These predictions capture seasonal and site-specific patterns, offering valuable insights into the expected distribution of seabirds in the CCS over longer time periods.

Relevance to Collision Risk Modeling

The 3D Framework is not a Collision Risk Model but rather a broad quantification of the spatial variability in the composition and magnitude of seabirds likely to fly at heights that would increase their potential to encounter RSZs and, consequently, their vulnerability to turbine-blade collision. The predictions provided by the 3D Framework, akin to passage rates, offer density estimates and flight-height information across the CCS, which are critical inputs for generating a formal Collision Risk Model. Such models aim to estimate the probability of a single bird colliding with a turbine blade upon entry into a RSZ and the likely number of collisions over a specific period (Band, 2012; Masden & Cook, 2016). Understanding flight heights is also important for generating accurate collision-rate predictions using a Collision Risk Model, particularly in determining whether a species flies at heights associated with collision risk. Thus, the predictions provided by the 3D Framework provide insight into the flight heights of various seabirds off CA, as well as an indication of the possible magnitude of passage at collision risk heights, including predictions for areas that may not otherwise have been surveyed.

During permitting and agency consultation, particular attention should be paid to small albatross, shearwaters (both diving and surface-feeding types), fulmars, and small and large gadfly petrels (not included in this analysis due to insufficient observations but well known to increase flight height with increased wind speed

(Ainley et al., 2015). These species tend to fly higher in strong winds and occur in the shelf break location near existing areas proposed for WEAs. Notably, all currently existing OSW facilities in the U.S. and Europe are positioned in relatively shallow water where the presence of these dynamic soarers (that fly > 10 m) is negligible. Therefore, it remains to be seen how they will alter their flight in the presence of turbines (e.g., by avoidance).

It should be noted that two federally listed species, the Hawaiian Petrel and Short-tailed Albatross, both of which are dynamic soarers, were not encountered in sufficient numbers in CA waters during the period covered by the surveys used in this analysis, in part due to their small population sizes. However, as a result of conservation efforts at breeding sites, both species have been increasing in the CCS in recent years, especially the Hawaiian Petrel, which is now a regular annual visitor in small numbers, primarily in continental slope waters. Short-tailed Albatross occurrence is far more sporadic. Both once had much larger populations (Carboneras et al., 2020; Simons & Bailey, 2020).

Recommendations and Future Directions

The 3D Framework, while a significant advancement, has certain limitations and areas for improvement that should be addressed by future research. For instance, the 3D Framework was constrained to seabird species detected often enough to occur within at least 100 km^2 of at-sea transect effort, resulting in the exclusion of species such as the listed Hawaiian Petrel and Short-tailed Albatross. These species are crucial to consider during permitting processes and should be incorporated into future iterations of the 3D Framework. Additional data limitations include: (1) observations were restricted to daylight even though seabirds do fly at night (Schneider et al., 2024); (2) survey timing may not have captured short-lived migration pulses because surveys provide 'snapshots' in space and time; and (3) aerial surveys were limited to low wind conditions. Additionally, it is difficult for human observers to see vertically across the full extent of the RSZ (up to 260 m ASL), and thus the flight-height data used in this study were based on conservative thresholds for flight in the RSZ. Although the 10 m ASL threshold between flight-height categories may appear conservative (given RSZs are typically 30 m ASL and higher), recent studies using new technologies off CA (Matzner et al., 2022; Schneider et al., 2024), indicate that most birds remain within the lowest 10 m of airspace. Nevertheless, some birds do fly at higher elevations that cannot be precisely resolved by observers categorizing individuals simply as "above 10 m." To overcome these challenges, future research should explore the integration of new technologies capable of detecting and identifying seabirds across the RSZ in varied environmental conditions and times of day. Projects funded by organizations like the CEC are actively developing such sensor technologies to address these limitations.

Methodologically, while the IDW spatial interpolation algorithm was ultimately employed for seabird 2D density estimates, other modeling techniques were considered but deemed impractical due to their inability to provide reasonable abundance estimates. Before settling on the IDW model approach to derive the seabird 2D density estimates, several other modeling approaches were attempted, including zero-inflated General Additive Models, Occupancy Models, and Kriging, with a suite of covariates (e.g., sea surface temperature, depth, distance to coast; similar to Leirness et al., 2021) to extrapolate observations to areas not surveyed. Ongoing refinement of modeling approaches is essential to enhance the accuracy of density predictions.

Future modification and use of the 3D Framework off CA could include incorporating newer at-sea observational data including efforts funded by BOEM and others. Observations from the past 10 or more years, as noted, indicate that some species have significantly changed in abundance (e.g., fewer Sooty Shearwaters, more Common Murres and Brown Pelicans), including historically rare birds that have increased in waters off CA (e.g., boobies). Some of the reasons for these changes include recovery of populations from protective measures at remote nesting sites (such as predator exclusion, in the case of the Hawaiian Petrel), reducing commercial fisheries bycatch (for albatross), and changing ocean conditions (for boobies).

The applicability of the 3D Framework extends beyond the CCS and can be adapted for use in other regions with sufficient observational data. The relationships between seabird flight behavior and wind speed, particularly > 10 m ASL, offer valuable insights that are applicable to a range of seabird species, including those uncommonly observed in the CCS (e.g., Hawaiian Petrel), for which FG characteristics are well understood and observations are increasing. Thus, ongoing efforts to refine and expand the 3D Framework will contribute to its broader utility in informing OSW development and environmental management strategies.

ACKNOWLEDGEMENTS

The authors would like to acknowledge several individuals that provided technical guidance, including Ryan Terrill (Klamath Bird Observatory) and Jerome Qiriazi (Humboldt Transit Authority). The members of the Technical Advisory Committee organized by CEC provided review of the manuscript and valuable input: David Pereksta (Bureau of Ocean Energy Management), Chris Potter (California Department of Fish and Wildlife), Garry George (National Audubon Society), Dan Barton (Cal Poly Humboldt), Kaus Raghukumar (Integral Consulting), Mike Optis (National Renewable Energy Lab), Yi-Hui Wang (Ocean Protection Council), Mark Severy (Pacific Northwest National Laboratory), Tyler Studds (Ocean Winds), and Brita Woeck (Ørsted). We thank the California Energy Commission for funding and support.

DISCLAIMER

This project was funded by the California Energy Commission. The content does not represent the official views of policies of the State of California. This report was created under agreement number: EPC-19-011

AUTHOR CONTRIBUTIONS

Conception: SRS, DGA, SBT, SHK, AJ, EW, CC; Data: CC, DGA, LTB, JAS; Data analysis: SRS, EW, SBB, ST, RGF, JC, CC; Interpretation: SRS, DGA, SBT, SHK, JAS, LTB; Writing: all authors.

REFERENCES

Adams, J., Felis, J., Mason, J. W., & Takekawa, J. Y. (2014). *Pacific continental shelf environmental assessment (PaCSEA): Aerial seabird and marine mammal surveys off northern California, Oregon, and Washington, 2011–2012* (OCS Study BOEM 2014-003). http://www.boem.gov/2014-003/

Adams, J., Kelsey, E. C., Felis, J. J., & Pereksta, D. M. (2016). *Collision and displacement vulnerability among marine birds of the California Current System associated with offshore wind energy infrastructure* (Open-File Report 2016-1154; OCS Study BOEM 2016-043). Bureau of Ocean Energy Management. https://www.boem.gov/sites/default/files/environmental-stewardship/Environmental-Studies/Pacific-Region/Studies/BOEM-2016-043.pdf

Ainley, D. G. (1976). The occurrence of seabirds in the coastal region of California. *Western Birds*, *7*(2), 33–68.

Ainley, D. G., & Boekelheide, R. J. (Eds.). (1990). *Seabirds of the Farallon Islands: Ecology, structure and dynamics of an upwelling system community*. Stanford University Press.

Ainley, D. G., & Hyrenbach, K. D. (2010). Top-down and bottom-up factors affecting seabird population trends in the California current system (1985–2006). *Progress in Oceanography*, *84*(3–4), 242–254. https://doi.org/10.1016/j.pocean.2009.10.001

Ainley, D. G., Dugger, K. D., Ford, R. G., Pierce, S. D., Reese, D. C., Brodeur, R. D., Tynan, C. T., & Barth, J. A. (2009). The spatial association of predators and prey at frontal features in the northern California Current: Competition, facilitation, or merely co-occurrence? *Marine Ecology Progress Series*, *389*, 271–294. https://doi.org/10.3354/meps08125

Ainley, D. G., McIver, W., Adams, J., & Parker, M. (2020). Ashy Storm-Petrel (*Oceanodroma homochroa*). In P. G. Rodewald (Ed.), *Birds of the world* (version 1.0.). Cornell Lab of Ornithology. https://doi.org/10.2173/bow.asspet.01

Ainley, D. G., Nettleship, D. N., & Storey, A. E. (2021). Common Murre (*Uria aalge*). In S. M. Billerman, P. G. Rodewald, & B. K. Keeney (Eds.), *Birds of the world* (version 2.0). Cornell Lab of Ornithology. https://doi.org/10.2173/bow.commur.02

Ainley, D. G., Porzig, E., Zajanc, D., & Spear, L. B. (2015). Seabird flight behavior and height in response to altered wind strength and direction. *Marine Ornithology*, *43*(1), 25–36. https://doi.org/10.5038/2074-1235.43.1.1098

Ainley, D. G., Spear, L. B., Tynan, C. T., Barth, J. A., Pierce, S. D., Ford, G. R., & Cowles T. J. (2005). Physical and biological variables affecting seabird distributions during the upwelling season of the northern California Current. *Deep-Sea Research II*, *52*(1–2), 123–143. https://doi.org/10.1016/j.dsr2.2004.08.016

Band, B. (2012). *Using a collision risk model to assess bird collision risks for offshore wind farms* (SOSS-02). The Crown Estate, Strategic Ornithological Support Services Programme. https://www.bto.org/sites/default/files/u28/downloads/Projects/Final_Report_SOSS02_Band1ModelGuidance.pdf

Bates, D., Machler, M., Bolker, B., & Walker, S. (2015). Fitting linear mixed-effects models using lme4. *Journal of Statistical Software*, *67*(1), 1–48. https://doi.org/10.18637/jss.v067.i01

Bograd, S. J., Schroeder, I., Sarkar, N., Qiu, X., Sydeman, W. J., & Schwing F. B. (2009). Phenology of coastal upwelling in the California Current. *Geophysical Research Letters*, 36, 1–5. https://doi.org/10.1029/2008GL035933

Bolin, R. L., & Abbott, D. P. (1963). Studies on the marine climate and phytoplankton of the coast of California 1954–1960. *California Cooperative Oceanic Fisheries Investigations Reports*, *9*, 23–45.

Briggs, K. T., Tyler, W. B., Lewis, D. B., & Carlson, D. R. (1987). Bird communities at sea off California: 1975 to 1983. *Studies in Avian Biology*, *11*, 1–74. https://doi.org/10.2307/4087784

Bureau of Ocean Energy Management (2022). *Pacific wind lease sale 1 (PACW-1) for commercial leasing for wind power in the Outer Continental Shelf in California: Proposed sale notice* (87 FR 32443). https://www.federalregister.gov/documents/2022/05/31/2022-11537/pacific-wind-lease-sale-1-pacw-1-for-commercial-leasing-for-wind-power-on-the-outer-continental

California Senate Bill 100, 2017–2018 Reg. Sess. (Cal. 2018). https://leginfo.legislature.ca.gov

Carboneras, C., Jutglar, F., & Kirwan, G. M. (2020). Short-tailed Albatross (*Phoebastria albatrus*). In J. del Hoyo, A. Elliott, J. Sargatal, D. A. Christie, & E. de Juana (Eds.), *Birds of the world* (version 1.0.). Cornell Lab of Ornithology. https://doi.org/10.2173/bow.shtalb.01

Checkley, D. M., & Barth, J. A. (2009). Patterns and processes in the California Current System. *Progress in Oceanography*, *83*(1–4), 49–64. https://doi.org/10.1016/j.pocean.2009.07.028

Chelton, D. B., Bernal, P. A., & McGowan, J. A. (1982). Large-scale interannual physical and biological interaction in the California Current. *Journal of Marine Research*, *40*(4), 1095–1125.

Clarke, E. D., Spear, L. B. McCracken, M. L., Marques, F. F. C., Borchers, D. L., Buckland, S. T., & Ainley, D. G. (2003). Validating the use of generalized additive models and at-sea surveys to estimate size and temporal trends of seabird populations. *Journal of Applied Ecology*, *40*(2), 278–292. https://doi.org/10.1046/j.1365-2664.2003.00802.x

Cook, A. S. C. P., Ward, R. M., Hansen, W. S., & Larsen, L. (2018). *Estimating seabird flight height using LiDAR*. Scottish Marine and Freshwater Science, 9(14). https://doi.org/10.7489/12131-1

Flint, S., deMesa, R., Doughman, P., & Huber, E. (2022). *Offshore wind development off the California coast: maximum feasible capacity and megawatt planning goals for 2030 and 2045* (Report CEC-8002022-001-REV). California Energy Commission. https://www.energy.ca.gov/publications/2022/offshore-wind-energy-development-california-coast-maximum-feasible-capacity-and

Ford, R. G., Terrill, S., Casey, J., Shearwater, D., Schneider, S. R., Ballance, L. T., Terrill, L., Tollefson, M., & Ainley, D. G. (2021). Distribution patterns and population size of the ashy storm petrel *Oceanodroma homochroa*. *Marine Ornithology*, *49*(2), 193–204. http://doi.org/10.5038/2074-1235.49.2.1424

Grémillet, D., Ponchon, A., Paleczny, M., Palomares, M-L. D., Karpouzi, V., & Pauly, D. (2018). Persisting worldwide seabird-fishery competition despite seabird community decline. *Current Biology*, *28*(24), 4009–4013. https://doi.org/10.1016/j.cub.2018.10.051

Harwood, A. J., Perrow, M. R., & Berridge, R. J. (2018). Use of an optical rangefinder to assess the reliability of seabird flight heights from boat-based surveyors: Implications for collision risk at offshore wind farms. *Journal of Field Ornithology*, *89*(4), 372–383. https://doi.org/10.1111/jofo.12269

Hickey, B. M. (1979). The California Current system: Hypothesis and facts. *Progress in Oceanography*, *8*(4), 191–279. https://doi.org/10.1016/0079-6611(79)90002-8

Howell, S. N. G., & Zufelt, K. (2019). *Oceanic birds of the world, a photo guide*. Princeton University Press. https://doi.org/10.1515/9780691197012

Joyce, T. W. (2016). *Foraging ecology, biogeography, and population biology of seabird and toothed whale predators in the Anthropocene*. [Doctoral dissertation, University of California San Diego]. https://escholarship.org/uc/item/0zp36438

Kelsey, E. C., Felis, J. J., Pereksta, D. M., & Adams, J. (2025). *Revised marine bird collision and displacement vulnerability index for U.S. Pacific Outer Continental Shelf offshore wind energy development* (Data Report 1214). Bureau of Ocean Energy Management. https://doi.org/10.3133/dr1214

Largey, N., Cook, A. S. C. P., Thaxter, C. B., McCluskie, A., Stokke, B. G., Wilson, B., & Masden, E. A. (2021). Methods to quantify avian airspace use in relation to wind energy development. *Ibis*, *163*(3), 747–764. https://doi.org/10.1111/ibi.12913

Leirness, J. B., Adams, J., Ballance, L. T., Coyne, M., Felis, J. J., Joyce, T., Pereksta, D. M., Winship, A. J., Jeffrey, C. F. G., Ainley, D., Croll, D., Evenson, J., Jahncke, J., McIver, W., Miller, P. I., Pearson, S., Strong, C., Sydeman, W., Waddell, J. E., … Christensen, J. (2021). *Modeling at-sea density of marine birds to support renewable energy planning on the Pacific Outer Continental Shelf of the contiguous United States* (OCS Study BOEM 2021-014). Bureau of Ocean Energy Management. https://espis.boem.gov/final%20reports/BOEM_2021-014.pdf

Li, B., Lingsma, H. F., Steyerberg, E. W., & Lesaffre, E. (2011). Logistic random effects regression models: A comparison of statistical packages for binary and ordinal outcomes. *BMC Medical Research Methodology*, *11*(77), 1–11. https://doi.org/10.1186/1471-2288-11-77

Masden, E. A., &. Cook, A. S. C. P. (2016). Avian collision risk models for wind energy impact assessments. *Environmental Impact Assessment Review*, *56*, 43–49. https://doi.org/10.1016/j.eiar.2015.09.001

Mason, J. W., Mcchesney, G. J., McIver, W. R., Carter, H. R., Takekawa, J. Y., Golightly, R. T., Ackerman, J. T., Orthmeyer, D. L., Perry, W. M., Yee, J. L., Pierson, M. O., & McCrary, M. D. (2007). At-sea distribution and abundance of seabirds off southern California: A 20-year comparison. *Studies in Avian Biology*, *33*, 1–101.

Matzner, S., Warfel, T. E., Hull, R., & Williams, N. (2022). *ThermalTracker-3D offshore validation technical report* (Contract DE-AC05-76RL01830). Pacific Northwest National Laboratory. https://tethys.pnnl.gov/sites/default/files/publications/PNNL-ThermalTracker-Offshore-Validation-2022.pdf

Midway, S. (2022). Random effects. In *Data analysis in R* (Chapter 9). https://bookdown.org/steve_midway/DAR/random-effects.html

National Renewable Energy Lab. (2023). *Wind toolkit data downloads: Offshore CA data download*. https://developer.nrel.gov/docs/wind/wind-toolkit/offshore-ca-download/

Nur, N., Jahncke, J., Herzog, M. P., Howar, J., Hyrenbach, K. D., Zamon, J. E., Ainley, D. G., Wiens, J. A., Morgan, K., Ballance, L. T., & Stralberg, D. (2011). Where the wild things are: Predicting hotspots of seabird aggregations in the California Current System. *Ecological Applications*, *21*(6), 2241–2257. https://doi.org/10.1890/10-1460.1

Paleczny, M., Hammill, E., Karpouzi, V., & Pauly, D. (2015). Population trend of the world's monitored seabirds, 1950–2010. *PLOS One*, *10*(6), Article e0129342. https://doi.org/10.1371/journal.pone.0129342

Pebesma, E. J. (2004). Multivariate geostatistics in S: The gstat package. *Computer and Geosciences*, *30*(7), 683–691. https://doi.org/10.1016/j.cageo.2004.03.012

Pebesma, E. J., & Wesseling, C. G. (1998). Gstat, a program for geostatistical modelling, prediction and simulation. *Computer and Geosciences*, *24*(1), 17–31. https://doi.org/10.1016/S0098-3004(97)00082-4

Pennycuick, C. J. (1987a). Flight of seabirds. In J. P. Croxall (Ed.), *Seabirds: Feeding biology and role in marine ecosystems* (pp. 43–62). Cambridge University Press.

Pennycuick, C. J. (1987b). Flight of auks (alcidae) and other northern seabirds compared with southern procellariiformes: Ornithodolite observations. *Journal of Experimental Biology*, *128*(1), 335–347. https://doi.org/10.1242/jeb.128.1.335

R Core Team. (2016). *R: A language and environment for statistical computing*. R Foundation for Statistical Computing. https://www.R-project.org/

Rose, A., Wei, D., & Einbinder, A. (2022). The co-benefits of California offshore wind electricity. *The Electricity Journal*, *35*(7), 107167. https://doi.org/10.1016/j.tej.2022.107167

Russell, T. M., Szesciorka, A. R., Joyce, T., Ainley, D. G., & Ballance, L. T. (2023). National Marine Sanctuaries capture enhanced abundance and diversity of the California Current Ecosystem avifauna. *Journal of Marine Systems*, *240*(1038887), 1–16. https://doi.org/10.1016/j.jmarsys.2023.103887

Schneider, S. R., Kramer, S. H., Bernstein, S. B., Terrill, S. B., Ainley, D. G., & Matzner, S. (2024) Autonomous thermal tracking reveals spatiotemporal patterns of seabird activity relevant to interactions with floating offshore wind facilities. *Frontiers in Marine Science*, *11*, 1346758. https://doi.org/10.3389/fmars.2024.1346758

Severy, M., Ortega, C., Chamberlin, C., & Jacobson, A. (2020). *Wind speed resource and power generation profile (California North Coast Offshore Wind Studies)*. Schatz Energy Research Center. https://schatzcenter.org/pubs/2020-OSW-R2.pdf

Simons, T. R., & Bailey, C. N. (2020). Hawaiian Petrel (*Pterodroma sandwichensis*). In A. F. Poole, & F. B. Gili (Eds.), *Birds of the world* (version 1.0.). Cornell Lab of Ornithology. https://doi.org/10.2173/bow.hawpet1.01.1

Spear, L. B., & Ainley, D. G. (1997a). Flight speed of seabirds in relation to wind speed and direction. *Ibis*, *139*(2), 234–251. https://doi.org/10.1111/j.1474-919X.1997.tb04621.x

Spear, L. B., & Ainley, D. G. (1997b). Flight behaviour of seabirds in relation to wind direction and wing morphology. *Ibis*, *139*(2), 221–233. https://doi.org/10.1111/j.1474-919X.1997.tb04621.x

Spear, L. B., Ainley, D. G., Howell, S. N. G., Hardesty, B. D., & Webb, S. G. (2004). Reducing biases affecting at-sea surveys of seabirds: Use of multiple observer teams. *Marine Ornithology*, *32*(2), 147–157. https://doi.org/10.5038/2074-1235.32.2.616

Spear, L. B., Nur, N., & Ainley, D. G. (1992). Estimating absolute densities of flying seabirds using analyses of relative movement. *The Auk*, *109*(2), 385–389.

Veit, R. R., McGowan, J. A., Ainley, D. G., Wahl, T. R., & Pyle, P. (1997). Apex marine predator declines 90% in association with changing oceanic climate. *Global Change Biology*, *3*(1), 23–28. https://doi.org/10.1046/j.1365-2486.1997.d01-130.x

Webb, A., & Nehls, G. (2019). Surveying seabirds. In D. M. Pereksta (Ed.), *Wildlife and wind farms, conflicts and solutions* (pp. 60–96). Pelagic Publishing. https://doi.org/10.2307/jj.29010223.7